DC Microgrid Energy Optimization

By

Muziwenkosi Jiyane
Student Number: 21408063

Submitted in fulfilment of the requirements for the degree of:

MASTER OF ENGINEERING
in the
DEPARTMENT OF ELECTRONIC AND COMPUTER ENGINEERING,

FACULTY OF ENGINEERING AND THE BUILT ENVIRONMENT

at the

DURBAN UNIVERSITY OF TECHNOLOGY

August 2024

Supervisor: Dr. N. Pillay
Co-Supervisor: Mr. R. Sewsunker

PREFACE

My name is Muziwenkosi Jiyane, and I am a Master of Engineering candidate at the Durban University of Technology, in the Department of Electronic and Computer Engineering. My research topic is “DC Microgrid Energy Optimization”. The topic was selected because most rural areas are geographically isolated. Since they are isolated, they do not have electricity infrastructure extensions in their areas because of the economical distance limitation. Microgrids offer a viable solution for meeting the power needs of rural areas. A significant amount of research has been done to optimize the operation of microgrids. This thesis contributes to that work by focusing on developing an energy management system using demand-side control of the microgrid. The microgrid was modeled and simulated in the MATLAB software.

This research aimed to design, model, and simulate a hybrid microgrid that will meet the needs of electricity in a selected area. The hybrid microgrid will consist of:

- A photovoltaic (PV) fuel cell (FC), and battery storage system to ensure a constant supply of power regardless of weather conditions.
- An energy management system that will optimize the energy generated to best meet the demand.
- A demand side management system (DSM) to observe the effect of a demand-side management system in the microgrid.

The introduction to the research topic and its background, aims, and objectives are provided in Chapter 1. This is then followed by Chapter 2, the literature review of the research study. Chapter 3 shows the development of the sizing and design of the microgrid system. Chapter 4 presents the model of the microgrid. Chapter 5 gives the simulated results of the designed microgrid system. Finally, Chapter 6 gives the conclusion and discusses recommendations to further the study.

I would like to thank my supervisor Dr. N Pillay and my co-supervisor Mr. R Sewsunker for their guidance throughout this work. I would also like to thank you, my reader: I hope you enjoy reading my thesis.

DECLARATION 1: SUPERVISOR

According to the contents of this thesis, as the candidates' Supervisor, I agree to the submission of the thesis.

Dr. N Pillay

(Main supervisor)

Date: 7 March 2025

Mr. R Sewsunker

(Co-supervisor)

Date: 7/03/2025

DECLARATION 2: PLAGIARISM

I, **Muziwenkosi Jiyane (21408063)**, the undersigned, declare that:

(i) The research reported in this thesis, except where otherwise indicated, is my original work.

(ii) This thesis has not been submitted for degree or examination at any other university.

(iii) This thesis does not contain other persons' data, images, graphs, or other information unless specifically acknowledged as being sourced from other persons.

(iv) This thesis does not contain other persons' writing unless specifically acknowledged as being sourced from other researchers. Where other written sources have been quoted, then:

a. their words have been re-written, but the general information attributed to them has been referenced.

b. where their exact words have been used, their writing has been placed inside quotation marks and referenced.

(v) Where I have reproduced a publication of which I am an author, co-author or editor, I have indicated in detail which part of the publication was written by myself alone and have fully referenced such publications.

(vi) This thesis does not contain text, graphics, or tables copied and pasted from the Internet unless specifically acknowledged and the source is detailed in the dissertation and the reference sections.

Muziwenkosi Jiyane

March 2024

DECLARATION 3: PUBLICATIONS

I, Muziwenkosi Jiyane (21408063) declare that the following publications came of this thesis.

i. M. Jiyane, N. Pillay, R. Sewsunker, "DC Microgrid Energy Optimization", International Conference on Electrical, Computer and Energy Technologies (ICECET), Cape Town, South Africa, 2023, pp 1-6, doi: 10.1109/ICECET58911.2023.10389540.

ACKNOWLEDGEMENTS

I am sincerely grateful to my supervisors, Dr. N. Pillay and my co-supervisor Mr. R. Sewsunker for their supervision and advice during my academic journey. Additionally, I want to thank everyone who contributed to the success of my research. I also want to express my gratitude to God for providing me with the knowledge and resources necessary to complete this dissertation despite all my challenges.

ABSTRACT

Microgrids that generate electricity using photovoltaic panels or wind turbines and batteries, provide a viable solution to meet low to moderate energy needs in rural, remote and informal settlements. However, these solutions are limited because they depend on the availability of sunlight or wind. To solve these limitations, researchers have proposed hybrid systems that combine multiple energy sources and can be more efficient than battery-powered photovoltaic or wind systems. These hybrid systems use dynamic dispatching to optimize the overall cost and performance of the microgrid. Energy management systems are widely used to achieve this dynamic energy distribution, including load profiling and intelligent decision-making for energy distribution. While many energy management systems focusing on automated demand side management have been deployed worldwide to optimize microgrids, less work has been done in South Africa.

This research is focused on designing a hybrid PV-driven battery and fuel cell backup system, initially concentrating on sizing the PV, battery, and fuel cell. The focus then shifts to developing an energy management system. The proposed system follows a low-power provision in a 48 VDC format, offering electricity for lighting, computing, entertainment devices, and communication modules. Seven rural households were chosen for the study, collectively consuming 8.64 kWh/day. The efficacy of the microgrid is examined with and without demand-side management and considering the impact of load scheduling. The findings revealed that reducing energy demand by the demand side led to an increase in current and output power due to the proportional relationship between current and power, while the bus voltage remained constant at 48V DC. Furthermore, an increase in loads resulted in a decrease in output power. The simulation was carried out using the MATLAB® Simulink™ environment.

TABLE OF CONTENT

LIST OF FIGURES

LIST OF TABLES

ABBREVIATION

AC	Alternating Current
BMS	Battery Management System
DC	Direct Current
DERs	Distributed energy Resources
DOD	Depth of Discharge
DR	Demand Response
EMS	Energy Management System
ESSs	Energy Storage Sources
EE	Energy Efficiency
FC	Fuel Cell
IC	Integrated Circuit
IGBT	Insulated gate bipolar transistor.
MGCC	Microgrid central controller
PWM	Pulse Width Modulation
MPP	Maximum power point
MPPT	Maximum power point tracking
MG	Microgrid
PV	Photovoltaic
PID	Proportional Integral Derivative
PECs	Power electronics convertors
P&O	Perturb and Observe
RESs	Renewable Energy Source
RE	Renewable Energy
SMPS	Switched-mode power supply
Wh	Watts hours

LIST OF CONSTANTS

A	Ampere
C	Capacitance
I	Current
Ic	Capacitor current
IF	Average forward current of the rectifier diode
VF	Forward voltage of the rectifier diode.
Iout	Output Current
I_{ph}	Photo current
I_{sc}	Short circuit current
I_{ip}	Input Current
ΔI	Ripple Current
V	Voltage
V_{oc}	Open circuit voltage
V_{in}	Input Voltage
V_o	Output Voltage
V_L	Voltage across inductor
V_c	Voltage across capacitor
ΔV	Voltage ripple
P	Power
L	Inductance
F_{sw}	Switching frequency
K_i	Short circuit current of cell at 25º Celsius and 1000W/W^2
T	Temperature (K)
T_n	Nominal temperature
G	Solar irradiation
q	Electron
n	the ideality factor of the diode

K	Boltzmann’s
E_{g0}	Band gap energy of the semiconductor.
N_s	Number of cells connected in series.
N_p	Number of cells connected in parallel.
R	Resistance
R_s	Shunt Resistance
V_t	Diode thermal voltage
Z	Impedance

Chapter 1 Introduction

1.1 Background

A large portion of rural areas are situated in geographically isolated locations [1]. Figure 1.1 shows a typical layout of rural isolated areas. Most isolated areas do not have grid infrastructure extensions to their areas due to economical distance limitation [2]. With the recent electrical shortage problems in South Africa [3], it would not be ideal to extend electrification grids to these areas. Furthermore, the combustion process of burning fossil fuels to drive steam generators contribute to global warming [4]. Adding more consumers to the existing grid would increase the usage of energy resources such as fossil fuels, which negatively impacts the natural environment due to the emission of Carbon Dioxide (CO_2) into the atmosphere [5, 6].

Figure 1.1. Geographical isolated rural area [1]

The use of renewable sources such as solar and wind presents a favourable solution to meet the need of electrical problems in isolated areas [7, 8]. Energy can be produced from the renewable sources locally, using sources that can perform better under that location weather conditions [9]. Rather than generating power in bulk using power stations which are located far away from consumers and using long-distance transmission lines to deliver energy to those isolated areas [10], it is possible to produce smaller units of power locally, from the renewable energy sources [11, 12]. Energy can then be fed back into the distribution network, or potentially consumed via localized distribution networks [13].

Figure 1.2 shows a typical example of an isolated geographical area and a microgrid has been used as means of power supply to the households. The microgrid demonstration plant, which provides power to the community of Wilhelmina farm in Ficksburg, Free State province in South Africa, was completed in November 2017. The community is made up of fourteen households and with a total community population of 81 inhabitants. The solar plant utilizes the suns energy and converts it to a maximum of 32 kW using solar panels [14].

Figure 1.2. Microgrid implemented in a geographical isolated rural area [14]

A system which depends on a single renewable energy source is possible, but not 100% reliable because it depends on the availability of the resource (sun or wind) [15]. When this resource is not available due to varying weather conditions then the system cannot sustain the consumer demands [16]. Energy storage sources such as battery and capacitor banks are usually added to the renewable energy system as an energy backup system during unfavourable weather conditions. This means that when there is sunlight, a portion of energy generated by the PV will be stored in batteries while the rest is fed to the loads. The stored energy is used when there is no sunlight or wind [17]. To store additional power that can last for few days, more batteries are required. However, more batteries will need more space which can be a limiting factor. In addition, battery replacement costs makes the solution expensive to store power for the short term [18, 19]. An additional source is needed that can provide power on demand for a longer term. Fuel cells can be a viable additional source to ensure availability of power when both the sun and batteries cannot supply consumers [20]. For this to be achieved, a management system needs to be implemented that will be in control of these energy sources to make sure that they are operated smartly and optimally.

1.2 Significance of the study

This research proposed a standalone DC microgrid by using PV, batteries, and fuel cells. An energy management system is proposed and simulated. The energy management system optimally deploys PV, battery, and/or fuel cell power and a demand side management was proposed since load demand plays a significant role in microgrids [21]. The most popular energy saving strategy that is currently implemented in South Africa on demand side is load shedding. The main disadvantage of load shedding is that it cuts power supply for the whole community for certain periods of hours. It's classified into stages. Stage 4 would normally cut power for up to 4 hours. There are currently no means of isolating critical appliances on feeders and only de energize noncritical appliances. There were nearly 3,800 hours of load shedding in 2022. With this research a development of a demand side energy management system will give analyses of how the microgrid would function under different energy demand conditions.

The DC system was proposed because it has significant advantages in solving some of the control issues inside a microgrid such as synchronization, and reactive power control. Low power consuming DC loads will be used because of their energy-efficiency over AC loads. DC also holds potential advantages in terms of reliability, efficient control, and simplicity in terms

of integration of renewable energy sources. 48 VDC bus lines were chosen because it is sufficiently high to supply appliances, and low enough not to cause serious harm to the human body.

1.2.1 Problem statement:

Renewable energy sources are gaining attraction as a first preference source of energy [7]. Their implementation does however, come with many challenges such as varying weather conditions and limited energy storage space. A microgrid system must address unreliability due to dependence on weather conditions, optimized power usage and decisions that promote longevity of the systems lifespan.

1.2.2 Research aims and objectives:

The aim of this research was to design, model and simulate a hybrid microgrid system that will meet the demands of consumer needs in a selected area and the objective of the research were:

i. To ensure constant supply of power regardless of weather conditions.

ii. To optimize the use of the energy generated to best meet the load demand.

iii. To develop a demand side management system which will impact on the overall system performance of the microgrid.

1.3 The thesis structure:

Chapter 2 provides a discussion on previous related work.

Chapter 3 presents the system calculations and fundamental system modelling.

Chapter 4 shows the complete simulation of the proposed system with the management control. Computer simulations highlight the different components that makeup the system such as, the

solar cells, PV arrays, maximum power point tracker (MPPT), DC to DC convert circuit, batteries, and finally the fuel cell systems.

Chapter 5 presents the results and analysis of the system.

1.4 Chapter summary

In summary, chapter 1 introduced the DC microgrid energy optimization research topic, where the background of the researchers was described. The discussion included the justification for this study, the current state of South African electricity supply, and potential solutions. Problem statement, research aim, and objective were presented in this chapter and the finally, the thesis structure provides the arrangement of the thesis.

Chapter 2 Literature Review

2.1 Introduction

Chapter 2 presents a literature review based on the research topic DC microgrid energy optimization. At the start of chapter 2, a brief historical review on renewable energy resources is discussed. A review of control strategies to optimize the microgrid then follows. Following this, the microgrid architecture is discussed, focusing on different types of microgrid architecture.

2.2 History on renewable resources

Renewable Energy (RE) is still a new field and growing rapidly. Sorensen was the first researcher to perform analyses on 100% RE [22]. He analysed 100% renewable energy systems in 1975 and published the first analyses on RE which was a case study based in Denmark [23]. Another researcher named Lovins became the second researcher to publish an article on 100% RE systems. The difference between Sørensen and Lovins publications was that Sørensen work was a quantitative analytic study while Lovins was based more on the major components of RE [24]. In 1996, Sørensen published another global academic analysis of a 100% RE system for the timeline till year 2050 [25]. In 2009, authors by the names of Jacobson and Delucchi [26] presented another analysis on 100% RE for the year till 2030. Jacobson and Delucchi work were focused on mostly solar and wind energy, which have zero carbon emission, unlike the previous authors whose work included fuels such as biomass and biogas [25].

In 2005, Czisch [27] in his dissertation proposed a 100% RE multi-node simulation in hourly resolution based on past weather data for a super-grid, targeting one billion population around the world. The study of Czisch was a breakthrough for more studies that followed on 100% RE super-grid and supported the ‘Desertec Vision’ of those years. The vision of Desertec focused on electricity production from renewable energy sources in a manner that protects the environment. In 2010, Heide and co-workers [28] derived the first optimal balance of solar PV and wind power for a 100% RE system for the case of Europe in hourly and high spatial resolution. They concluded that 45% solar PV and 55% wind power would be optimal. Using this stylized approach, known as weather-driven modelling, they described the impact of

assuming different wind and solar combinations and heterogeneities among the European countries. They evaluated the impact of extending transmission links and storage [22, 28].

In 2009, another breakthrough on electrical power conversion to chemical was achieved by Sterner [29]. Sterner used a process of CO_2 reduction using hydrogen, his main source of CO_2 was biomass. Converting power to gas has been a much-needed breakthrough in the industry as it paves the way for hydrogen storage. By 2014, an Open Energy Modelling Initiative was formed. Its goal was to achieve transparency in RE modelling. This allowed for many researchers to exchange knowledge within the study of 100% RE [22]. During the period of 2017 to 2021, Bogdanov and co-workers [30] developed a new standard in global and local transition studies to 100% RE using the LUT-Energy System Transition Model (LUT-ESTM). It modelled the world in 145 individual regions at full hourly resolution with multi-node optimization using different regional and country schemes and for the entire energy industry system. This modelling framework also includes comprehensive electricity and chemical sector linkages across approximately 120 technologies across all sectors and industries. [31].

Nuclear and fossil fuel still dominate the energy industry, with the study shown in Germany [32] that even by 2030, these two non-renewable energy sources will still be dominating the energy sector [33]. More studies are done on RE and the changing models allows for the integration of energy system coupling and larger study areas with increased spatial and temporal resolution and the transmission grid [34]. Energy system models must be combined with more detailed energy system simulations for each synchronously operating system to demonstrate the viability of energy and power systems with future wind and solar resources [35]. The first steps of 100 % RE were often to convincingly demonstrate to stakeholders that renewables can replace fossil fuels, especially coal and nuclear power plants with high utilization rates. Much has been done to achieve that, but considerable research is required until 100% RE completely replaces fossil fuels.

2.2.1 Solar energy

The history of solar cells dates to 1839, where the French scientist Alexander Edmund Becquerel was working on metal electrodes in an electrolyte solution when he saw that current was created by this metal when the sun shone on them [36]. From 1839 to 1954, solar cells were

developed but were less effective until 1954, when Bell laboratories demonstrated the first silicon solar panel. This panel was 6% effective in converting sunlight to electricity. [37]. This was a significant improvement comparing the silicon solar panel to the selenium solar panel, which was made in 1883 by Charles Fritts which was less than 1% in converting the sunlight to electricity [38]. At that time, the silicon solar cells were very expensive to manufacture and were initially used to power satellite Nimbus spacecraft in 1964 [39]. With time, the production of silicon cells was simplified, making them less costly to manufacture. Figures 2.1 and 2.2 show the improvement in efficiency from 1995 to 2020 [37].

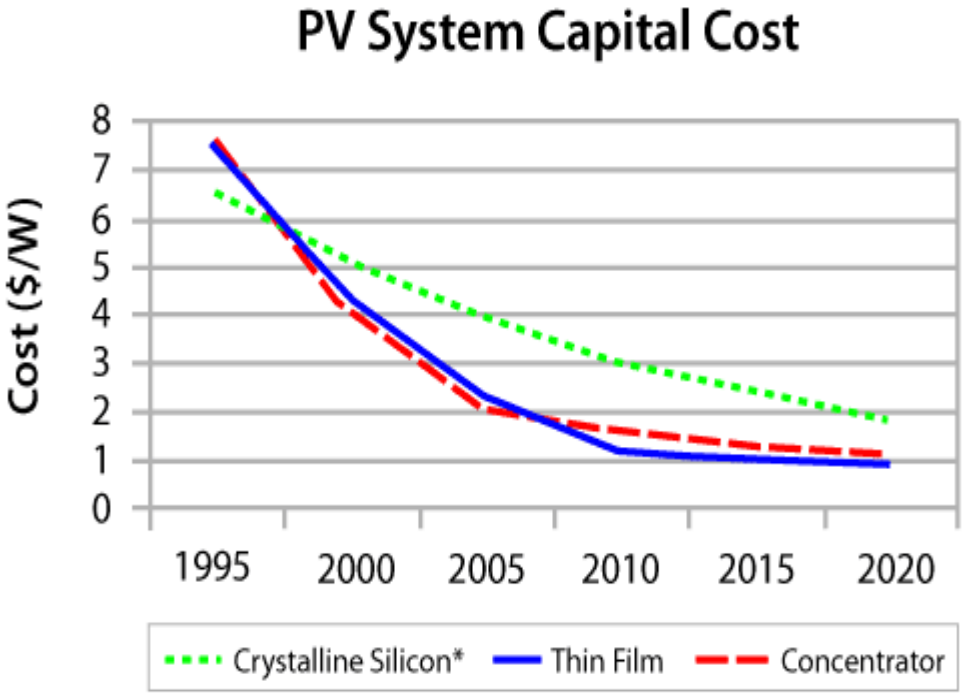

Figure 2.1. PV system capital cost [40]

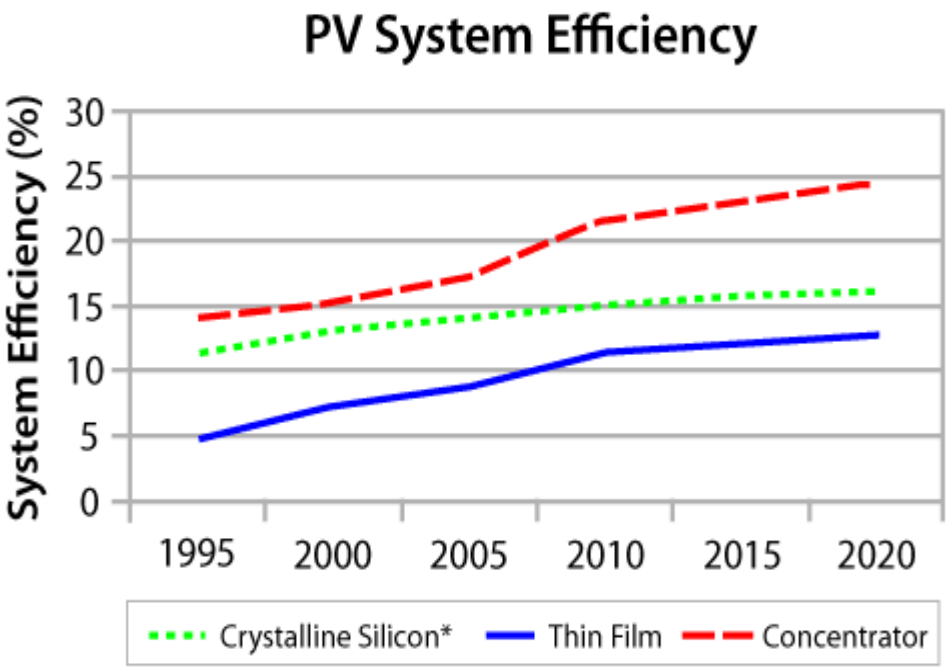

Figure 2.2. PV efficeincy [40]

The simplest solar cell form can be represented by Figure 2.3. A diode parallel to an ideal current source can characterize electrical energy. The current delivered at the output is proportional to the flux of insolation the solar cell receives. A solar cell produces about 2W at approximately 0.5V DC. To increase the solar cell power and voltage, single solar cells are connected in series or parallel or combination of parallel and series to achieve the desired voltage and power on a single module.

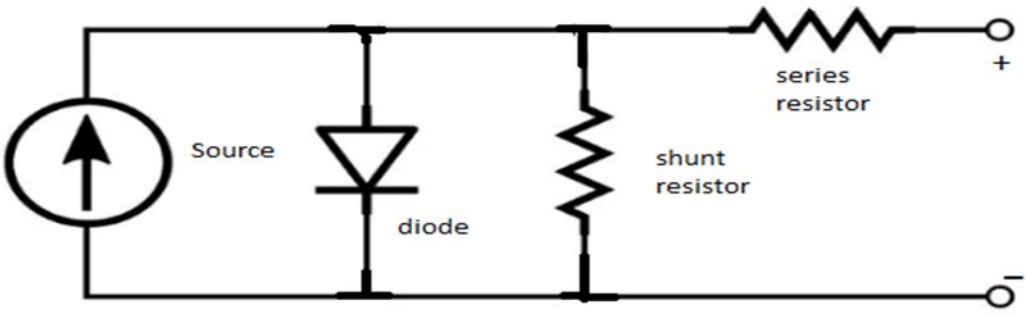

Figure 2.3. Solar cell equivalence circuit diagram

2.2.2 Wind turbines.

In simple terms, wind turbine uses air movement to generate electrical energy. Unlike solar energy, which generates DC power, wind turbine generates AC power. In 1883, one of the first wind turbines was installed as means of generating electricity at the Vienna International Electrical Exhibition by Josef Friedländer [41]. Figure 2.4 shows the first installed wind turbine for generating electricity. While this was the first wind turbine installed for generating electricity, wind turbines date back to 1883. The first documented wind turbine is the Persian windmill in 644 AD as shown in Figure 2.5 [42]. These wind turbines were mainly used for water pumping, driving sailboats, and grinding grain.

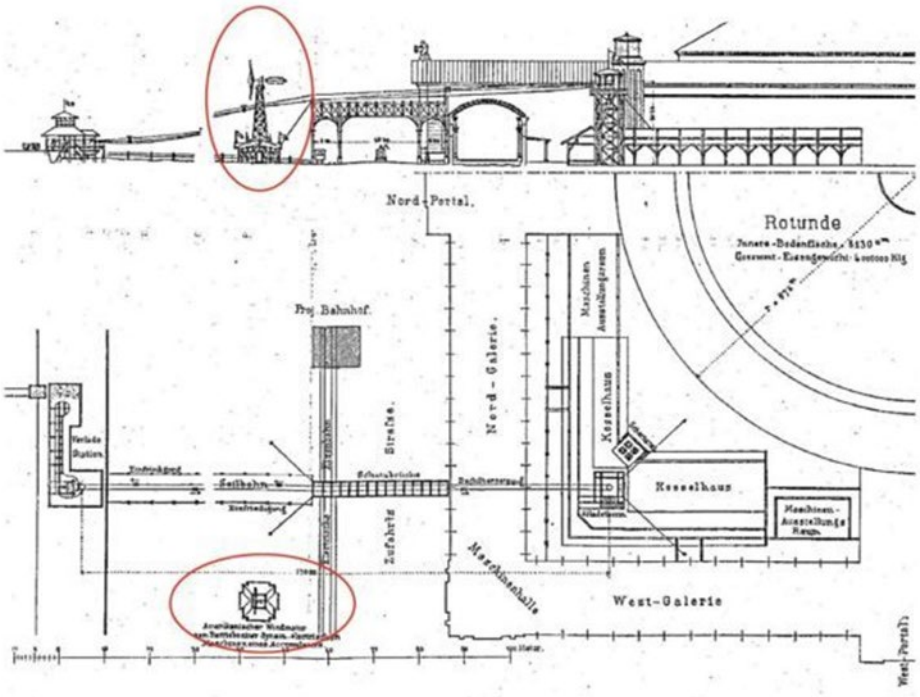

Figure 2.4: The first wind turbine installed in 1883 [41]

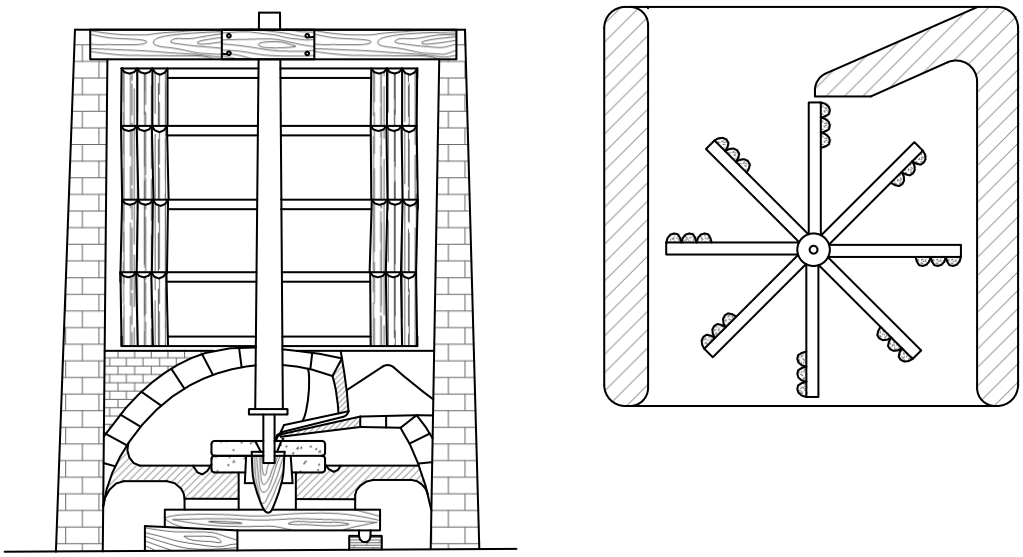

Figure 2.5: Persian windmill [42]

With advancements in technology, wind turbines also advanced from being used to pump water in agricultural applications to power lights for buildings in remote areas [43]. Several wind turbine farms suitable for small and large-scale farms have been developed over the years. Larger scale wind turbines have also been developed and linked with existing grids for remote use of power. Wind-powered generators operate in sizes ranging between small plants for battery charging at isolated residences up to gigawatt sized offshore wind farms that provide electricity to the national electrical network. Over the years, electricity generation from wind turbines has increased. Figure 2.6 shows the energy generated from a wind turbine from 2001 to 2020. The wind power generation began in 2001 where the power generated was 24 GW to 2020 which escalated to 792 GW. This is a significant increase moving towards 100% RE sources.

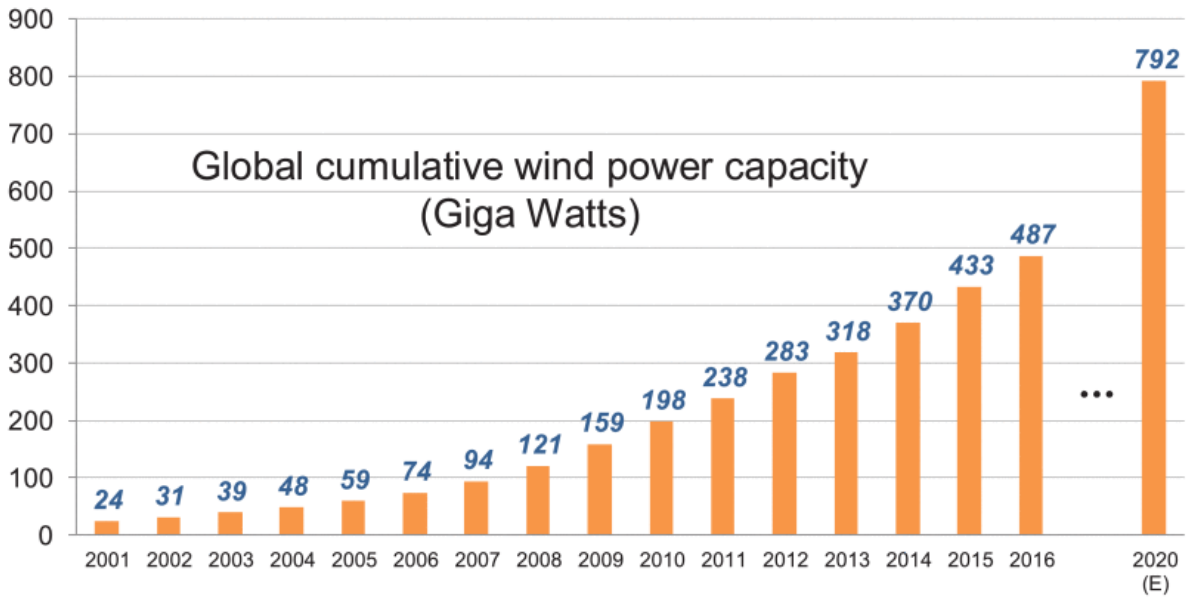

Figure 2.6: wind turbines cumulative power capacity over the years [44]

2.2.3 Hydrogen energy

A fuel cell is an electrochemical unit that converts a chemical reaction into electricity. Fuel cells require a continuous source of hydrogen and oxygen to sustain the chemical reaction and produce electricity. The fuel cell can be described as a battery that lose energy if hydrogen and oxygen are present to create a chemical reaction. In 1838, Sir William Grove [45] invented the first fuel cell, but it took centuries before it became commercially available. NASA used the fuel cell in the 1960s to power satellites in space. The fuel cell that National Aeronautics and space administration (NASA) used was the hydrogen-oxygen fuel cell, which was invented by Francis Thomas Bacon in 1932 [45]. Over the years, fuel cells have grown to be used in various applications in the transportation industry. Figure 2.7 shows a typical fuel cell's chemical reaction consisting of an anode, a cathode, and an electrolyte that allows ions to flow. Positively charged hydrogen ions, known as protons, move between the two sides of the fuel cell. A catalyst speeds up a chemical reaction, causing the fuel to undergo oxidation reactions that generate ions and electrons. The ions move from the anode to the cathode through the electrolyte. At the same time, electrons flow from the anode to the cathode through an external circuit, producing DC electricity.

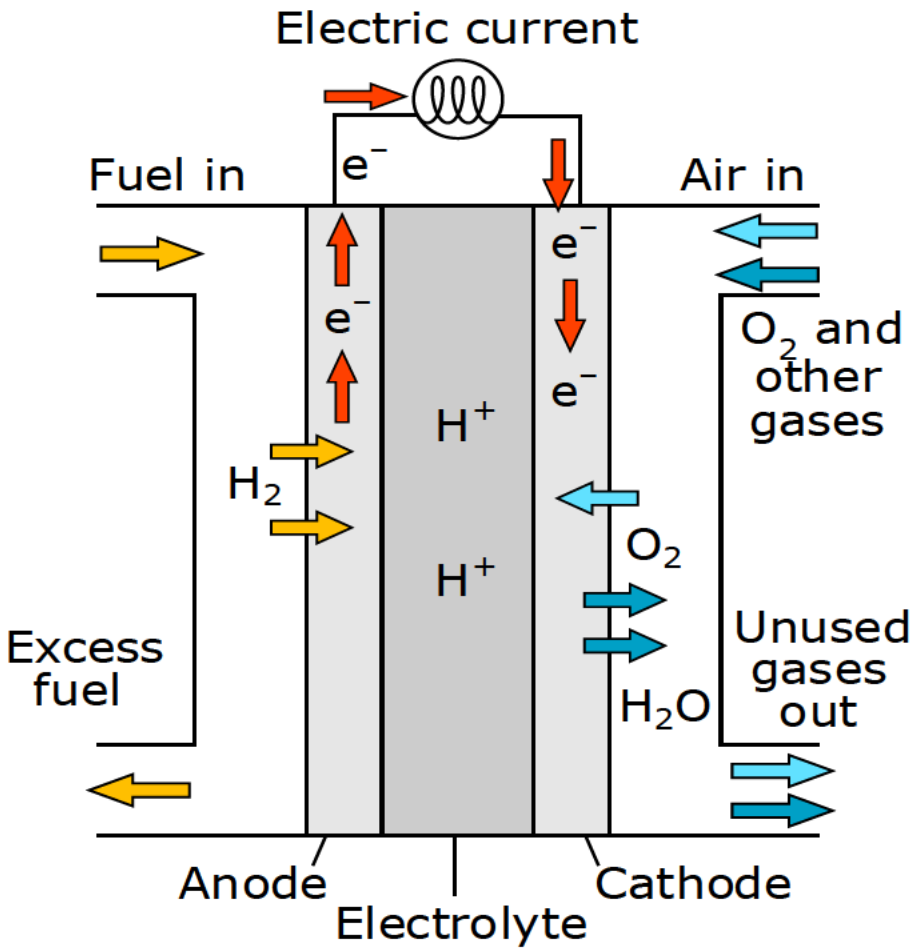

Figure 2.7. Fuel cell chemical reaction [46]

2.3 A review on optimization strategies

This literature review section discusses several microgrid optimization strategies studied and developed by different researchers. Many optimization strategies are available to optimize the operation of the microgrid. The optimization strategies are designed based on the factors that affect the microgrid's ability to operate at its optimum level. Some factors that affect the microgrid are the location of the microgrid, which will determine the type of renewable resources best suited for that location, and microgrid architecture. Many strategies can be used to implement and optimize microgrids. One such strategy is a Model Predictive Control (MPC)

algorithm. MPC is a control strategy used in linear and nonlinear systems. This strategy is based on the optimal control theory by Camacho and Bordons [47]. Figure 2.8 shows the diagram of the MPC, the prediction model, two manipulated inputs, disturbances, and output information (states as measured variables) to compute the future estimated states.

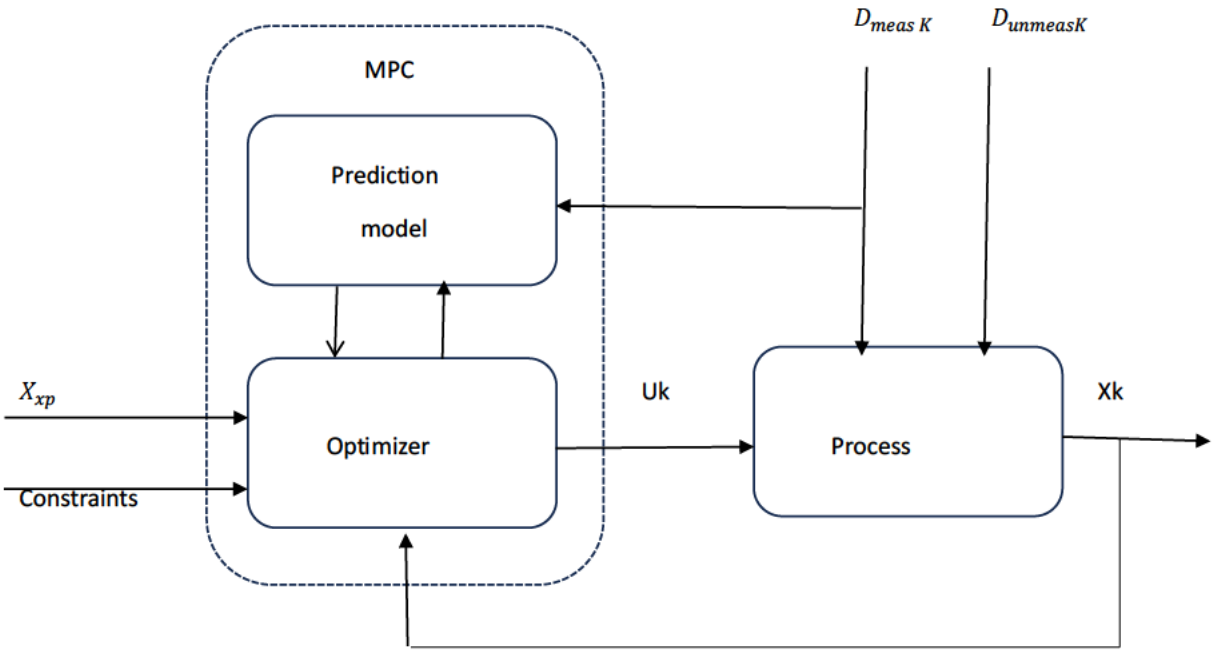

Figure 2.8: Model prediction control strategy

In the research conducted by Sunny and Thomas [48], they discussed and implemented a synchronized energy management system using a nonlinear model predictive control (NMPC) algorithm. This method makes the wind turbine and a PV array of a standalone DC microgrid as controllable power generators by adjusting the switching duty cycles of converters [48]. Sunny and Thomas objective was to determine the stability of DC microgrid that can be obtained from the stability of dc bus voltage level. The authors concluded that the controller could achieve the constant current and voltage required, for example, in charging battery cells. The changing load demands can be accurately shared between corresponding generators. Sunny and Thomas's work relates to the research as both works focus on optimizing the energy on a

microgrid. For this research, a different strategy is used to implement an energy management system with a power management system [49, 50].

Another control strategy that can have been used to optimize microgrid operation is the active and reactive power (PQ) control. This optimization strategy aims to achieve constant output power or voltage. Prasenjit Basak et al., 2009 presented a paper in which they discussed and presented control techniques required for microgrid operation. They implemented a simple control strategy of a microgrid model realized with MATLAB® [51]. They aimed to regulate voltage and frequency and keep these values within acceptable limits for a simulated microgrid. Their control strategy is PQ control, by controlling the microgrid source so that its real and reactive power are constant. This research requires a 48V DC bus voltage from the energy sources to power the loads. A Proportional and Integral (PI) control is used than PQ control strategies because of its simplicity. The PI controller controls the DC-DC convertor circuit to ensure a constant DC voltage across the DC bus voltage [52].

E. Natsheh [53], in his dissertation performed a simulation on a hybrid system using Artificial Neural Network (ANNs) to implement a MPPT using an advanced Fuzzy Logic Control (FLC) algorithm for the distribution and control of the charging of the batteries [53]. He then compared the FLC algorithm to the linear method called perturb and observe (P&O) algorithm and observed its effect on the two methods for improving battery charging. For this research, a different approach will be taken when simulating a hybrid system energy management and maximum power point controller unit. The energy management system will not only focus on battery charging and discharging. It will also be responsible for the power distribution, load controlling and mode of operation. The main purpose of the management system is to optimize the microgrid [54, 55].

Ferruzzi and Graditi [56] published a paper on the demand side to optimize residential microgrids. The paper discussed demand side management (DSM) using shifting techniques. In this methodology, the microgrid is governed by a prosumer, a decision maker who manages distributed energy sources, storage units and associated loads in the grid system [56]. DSM is considered an integral part of the optimal economic short-term management problem such as the allocation of shiftable loads. It is treated as a variable which must be determined simultaneously with all the other variables including energy exchange within the main grid.

Their paper focused on the formulation of a technical model, including functional links between moveable and shifted loads [57].

Many strategies have been designed and implemented to optimize the operation of standalone DC microgrids. As microgrids gains popularity, as apparent by the number of research being done. Different strategies are being proposed to implement microgrid control and optimization. This research will contribute to the field of study by implementing and optimizing a DC microgrid to supply electricity to a small rural community comprising of seven households. Using three different RE sources, the operation of which will be controlled by an energy management system.

2.4 Microgrid architecture

Based on their voltage characteristics and system architecture, microgrids can be categorized into three distinct types: DC microgrids, alternating current (AC) microgrids, and hybrid AC/DC microgrids, [58, 59]. These classes are discussed in subsequent sections.

2.4.1 AC microgrids

The most common type of microgrid is the AC microgrid shown in Figure 2.9. Power Electronics Convertors (PECs) are used to integrate various Distributed Energy Resources (DERs), such as fuel cells, wind turbine generators, microturbines, and solar photovoltaic systems, into a power network [60]. Since traditional power networks run on AC supply, the AC microgrids require the fewest adjustments to integrate with the current utility grid [61]. Due to their connectivity to low and medium voltage distribution networks, AC microgrids have the potential to reduce transmission line power losses and improve power quality in distribution networks. However, they have the inherent disadvantages of reactive power, DER synchronization, power quality, and system stability issues [62, 63]. Figure 2.8 shows an example of a typical AC microgrid configuration.

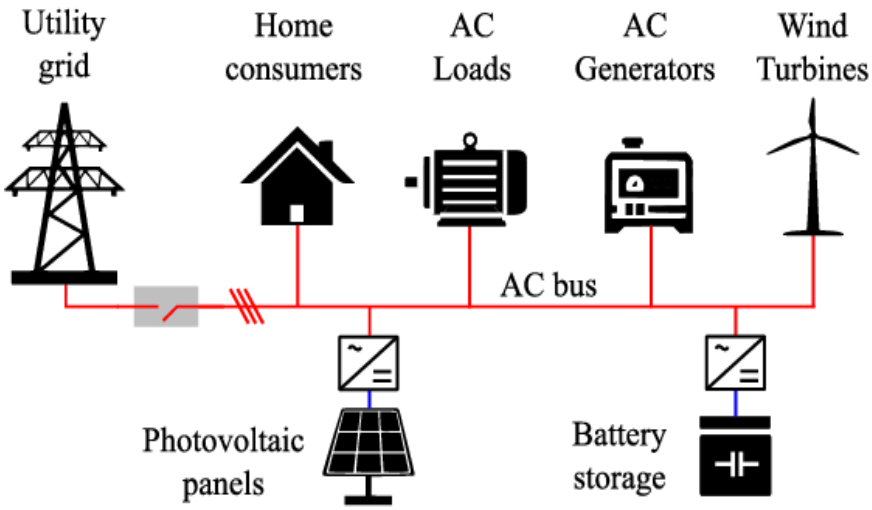

Figure 2.9. AC microgrid configuration [64]

2.4.2 DC microgrids

The DC microgrid provides energy savings by reducing the number of converters inside the microgrid system. This includes converters for interfacing the distributed renewable generations, loads and energy storage devices as shown in Figure 2.10. Numerous DC loads and power converters have been employed for various purposes due to advancements in PEC technology [65]. Furthermore, various ESS types and DC-based DERs open new possibilities for DC microgrids. Approximately 30% of the generated AC power goes through a PEC on average before being used [66]. This means that the number of power conversion stages is reduced [67].

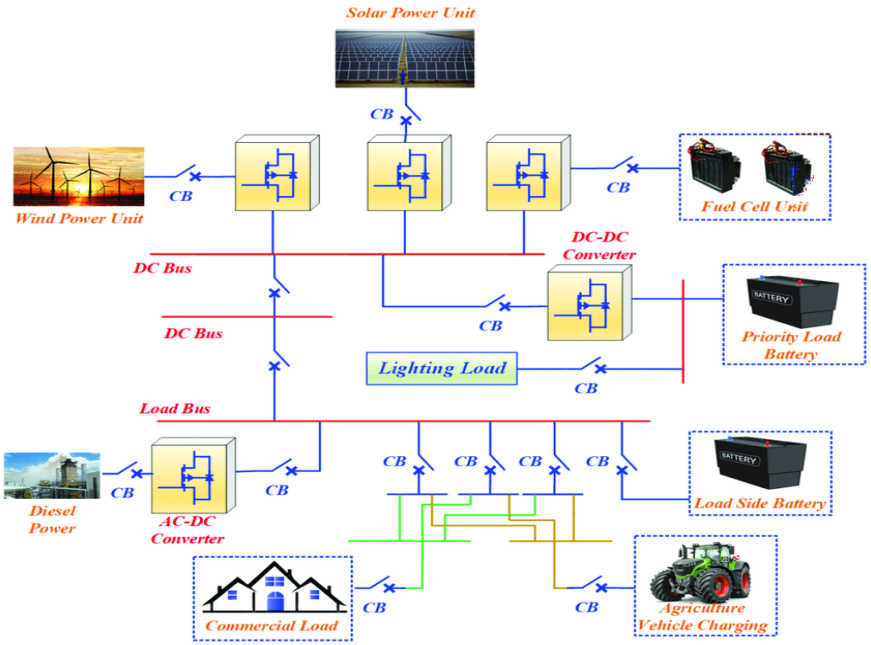

Figure 2.10. DC microgrid configuration [67]

2.4.3 Hybrid AC/DC microgrids

A hybrid AC/DC microgrid is formed by combining the two types of microgrids as shown in Figure 2.11. It provides significant advantages in terms of higher efficiency and dependability. The hybrid AC/DC microgrid makes direct integration of AC and DC-based DERs, energy storage sources (ESSs), and loads with the current distribution system possible. [68]. Hybrid AC/DC microgrids result in lower power losses. Furthermore, compared to the rectifier, the inverter experiences less power losses. [69, 70]. Hybrid AC/DC microgrids have a complicated structure due to the effect of their intermittent nature and the coordinated control of individual AC and DC microgrid structures [71].

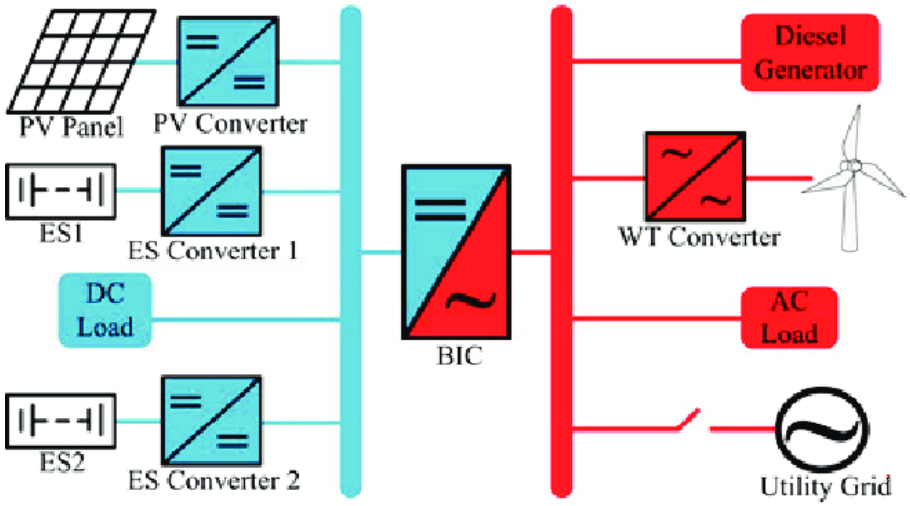

Figure 2.11. AC/DC microgrid configuration [72]

2.5 DC microgrid architecture

Different DC microgrid architectures are possible and their architectures have been reported recently [73]. This section discusses DC microgrid architecture schemes in detail, including their applications, advantages, and disadvantages.

2.5.1 Radial configuration

In the radial configuration scheme, the DC bus is connected to an AC grid at one end, and power flows in a single line to the loads. Only one line is available between each load to the AC grid interface [74]. Figure 2.12 shows a typical example of radial configuration. A single-line diagram of the radial DC microgrid system where a few renewable energy resources (RES), energy storage system (ESS), and loads (both AC and DC) are connected to the DC bus. This bus can be unipolar or bipolar, depending on applications and requirements. This configuration can be used in buildings where the low-voltage DC bus is preferred to match the voltage level of many appliances and to avoid unnecessary DC-DC conversion stages [75].

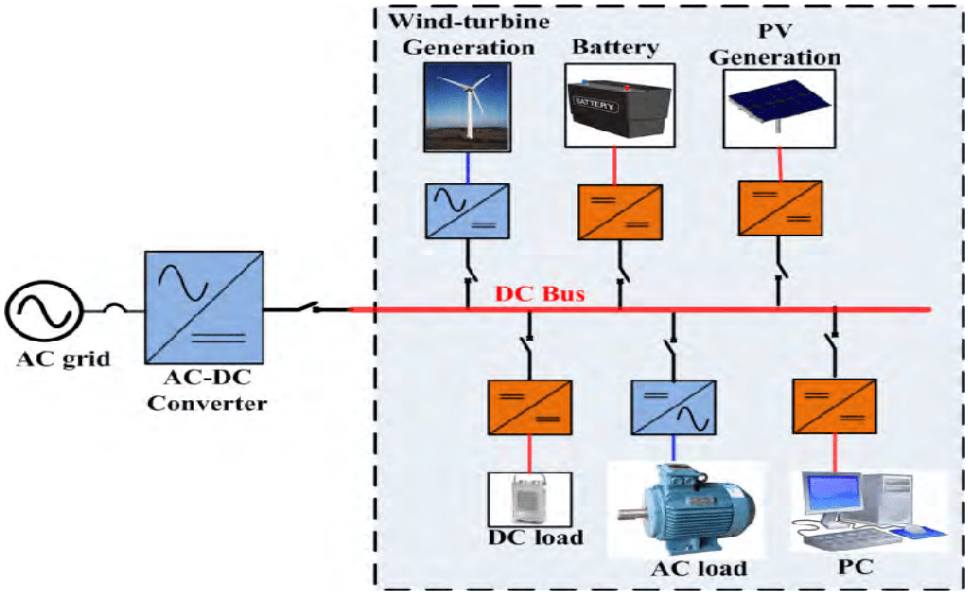

Figure 2.12. Radial Configuration [76]

2.5.2 Ring configuration

In the configuration shown in Figure 2.13, the AC grid interface and the customers are connected by two or more lines. Urban and industrial settings can use this kind of distribution system [77]. Although both ring and radial microgrid systems rely on the AC grid supply, the ring-type distribution system is more dependable than the radial system. The DC microgrid system cannot receive the necessary supply from the AC grid when an issue arises with the AC feeder [78].

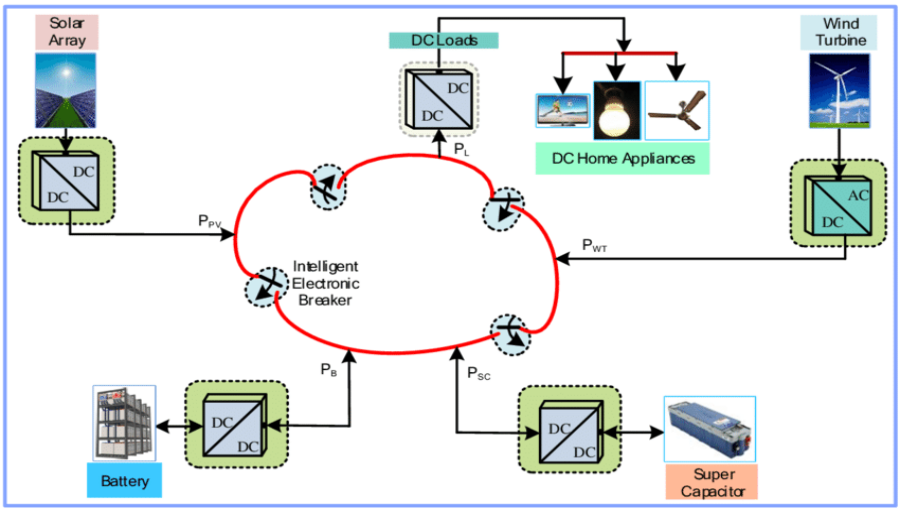

Figure 2.13. Ring Configuration [76]

2.5.3 Interconnected configuration

If one or more sources fail, the DC microgrid system can be improved by connecting an alternative AC grid supply to the users [79]. This can be done by interconnecting the DC bus with more than one supply from the AC grid. Two types of architecture can be constructed in this scenario, briefly discussed in the following sections.

i) Mesh Type DC Microgrid System

In a mesh-type DC microgrid, more than one AC grid interface is connected to the DC grids, each through an AC-DC converter. This configuration connects several DC and AC power supplies to the DC feeders [76] . Figure 2.14 shows an example of a mesh-type DC microgrid configuration.

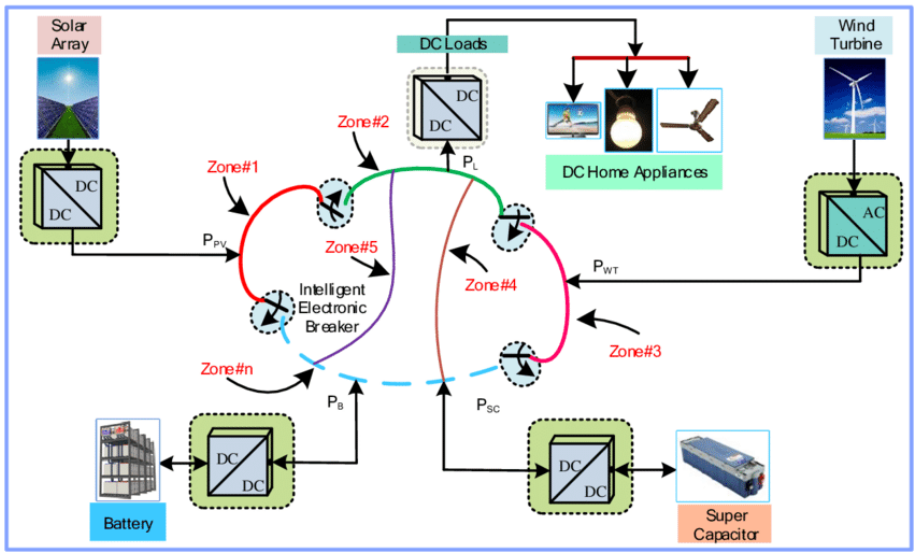

Figure 2.14. Mesh-type DC Microgrid [80]

ii) Zonal Type DC Microgrid System

The Zonal Type DC Microgrid System (ZTDC) shown in Figure 2.15 contains several power systems elements, such as power electronic converters, ESS, and switchgear, to supply a group of loads. Each zone relates to two redundant DC buses powered by the AC grid and distributed DC and AC energy sources. This type of architecture provides better reliability and availability for the loads that can be supplied through one of the energy sources.

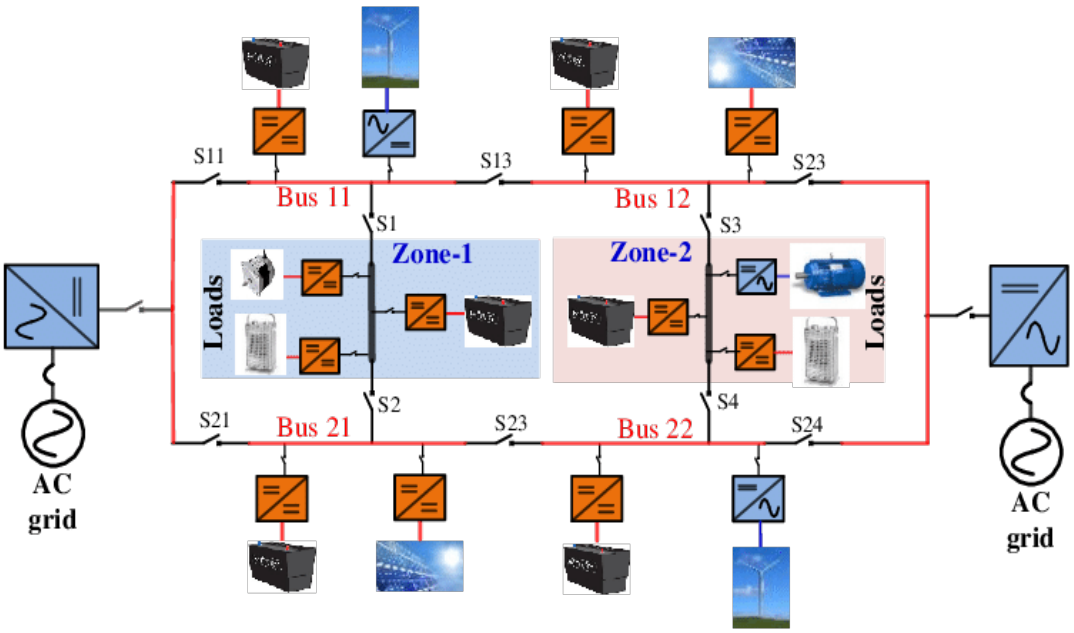

Figure 2.15. Zonal-type DC Microgrid [76]

2.6 Chapter summary

A discussion of solar, wind turbines, and fuel cells was given. After the discussion on 100% RE sources, control strategies that other researchers have implemented were reviewed and described. Different microgrid configurations were discussed. A radial DC configuration was selected as it reduces energy dissipation and facility costs from AC/DC conversion. Finally, the use of a DC microgrid increases the overall system's stability, reliability, controllability.

Chapter 3 Methodology

3.1 Introduction

Correct sizing of microgrid parameters is critical as it ensures that the microgrid operates effectively and efficiently to satisfy the load demands [80]. This chapter focuses on the methodology used to size each component and its proposed controlled strategy.

3.2 System design block diagram

The proposed microgrid system is illustrated in Figure 3.1 block diagram. The block diagram consists of two energy sources (solar and fuel cell systems) and one storage source, namely the battery. Power flows from the energy source to the DC-DC converters, where it is controlled. From the converters, the power is combined with the energy management system and fed to the household.

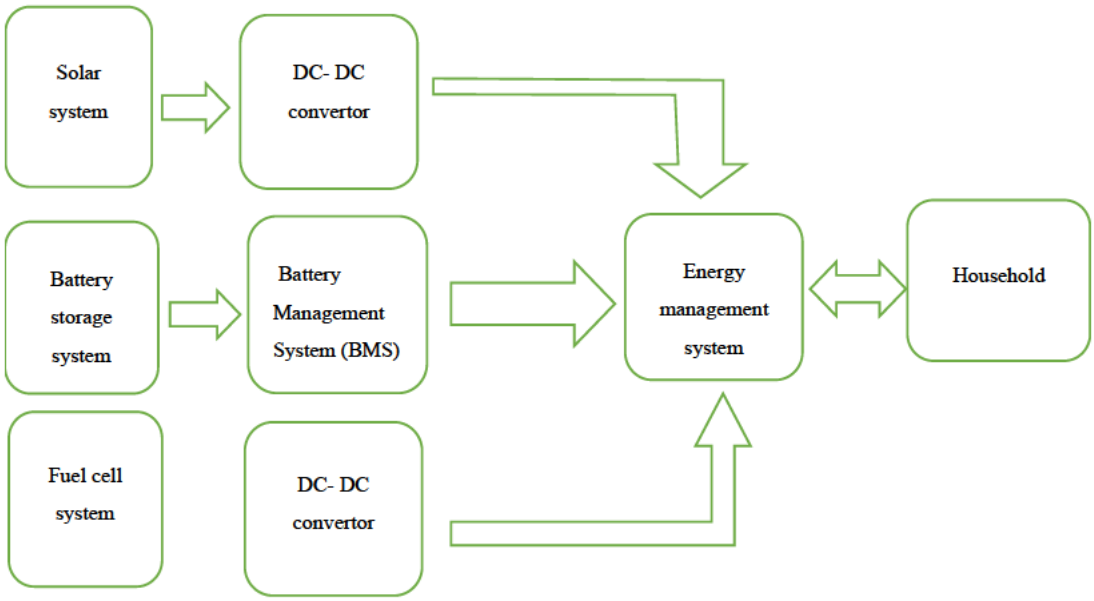

Figure 3.1. System block diagram

3.3 Load profiling

The first step when selecting a microgrid energy source is to look at the local weather conditions where the microgrid will be constructed. For this research, the chosen location is a rural area near Pietermaritzburg, Kwa-Zulu Natal Province in South Africa. The chosen location has a sample size of seven households. In the selected location, Table 3.1 shows a list of appliances that consume low energy and are commonly available to consumers. It provides the power rating of each appliance and the number of hours it is used. These appliances were chosen to minimize energy usage and include LED lighting instead of traditional fluorescent tubes. A 30W LED light will produce the same amount of lighting as a 60W fluorescent light, reducing total microgrid size [81]. Other sources may be used to power high-energy-consuming appliances, such as gas stoves and solar-powered geysers for heating.

Table 3.1. Low energy-consuming appliances for the selected location

Type of appliance	**Usage per day (hours)**	**Combined rated power (Watts)**	**Energy consumption (kWh)**
TV/Mobile/PC	10	450	4.5
Lights	7	610	4.27
Other	3	30	0..09
Total	**20**	**1090**	**8.86**

The selected load energy consumption rate was monitored over a period of 12 months and a daily hourly average of energy consumption was recorded. The loads were classified into critical and non-critical loads [82, 83], of which the essential loads were those that need power all the time and non-critical were those that can be disconnected from the grid when high energy demands are experienced. These loads can be potentially disconnected during the emergency case to preserve balance in the microgrid. Furthermore, critical loads had high priority over

non-critical loads. As shown in Figure 3.2, the consumer's energy usage was recorded and plotted on an hourly distribution graph. The graph shows the high and low peak energy demand. Furthermore, the data shows a high peak in the morning due to lighting and other activities. In the midday, the energy usage drops because most energy users are at work. However, in the evening, the energy usage starts to rise as most people return home and more electrical appliances are being utilized. From Figure 3.2, it was observed that from 4:00 to 9:00, there is a high energy consumption. From 10:00 to 14:30, the energy usage drops to the low peak of around 0.25 kWh. The graph reaches a peak of 0.7 kWh at approximately 18:00 each day. From 22:00 to 3:00, the energy usage drops as people sleep, turning off indoor lights and televisions.

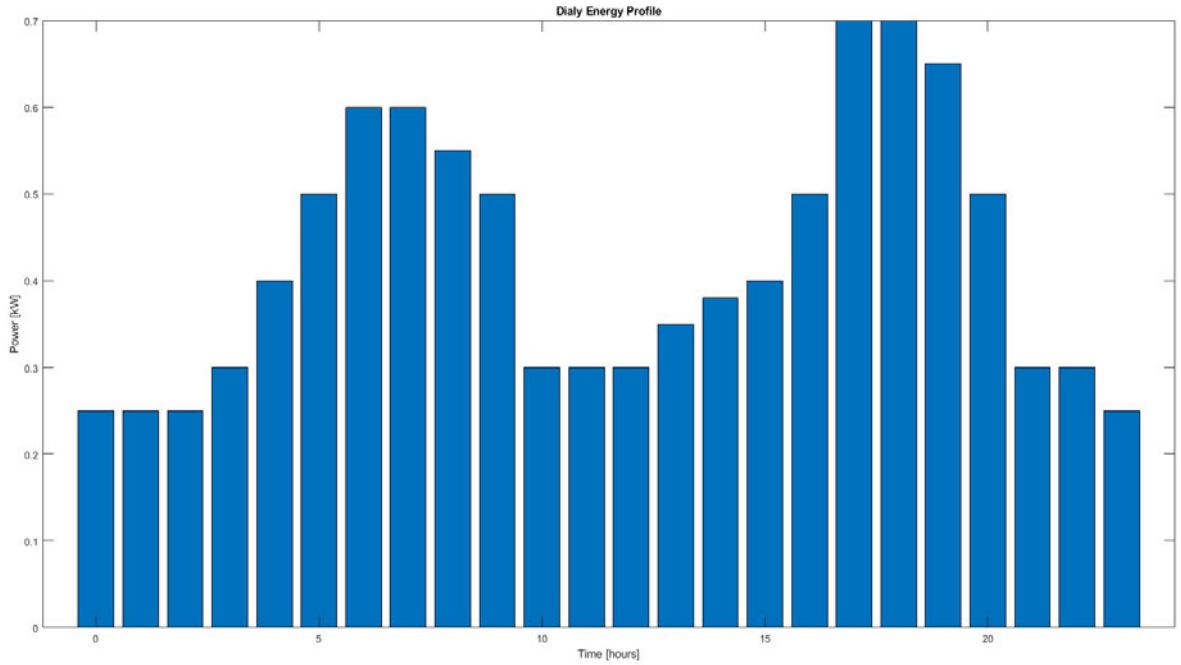

Figure 3.2. Load profiling for seven rural households per day.

Figure 3.3 shows the energy profile simulation results using 'Homer®' energy software. The results of the daily energy profile in Figure 3.2 are then compared to Figure 3.3. The two daily profile figures are similar.

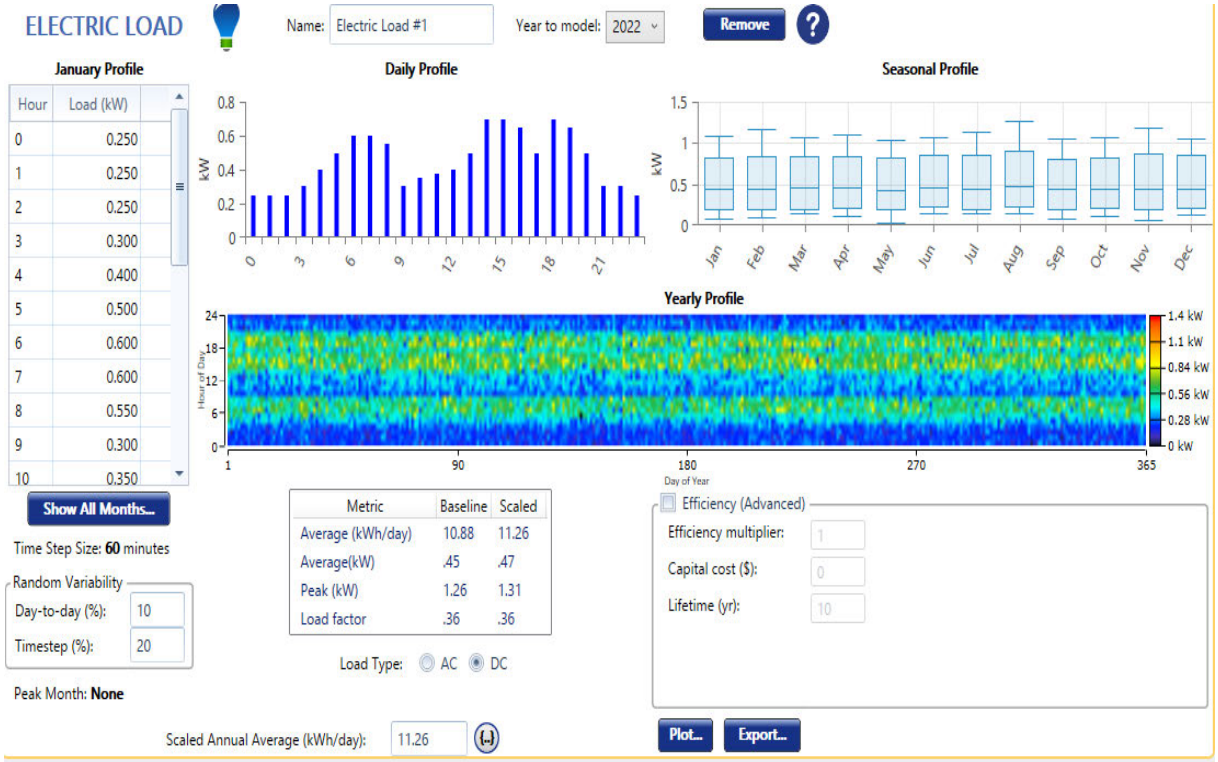

Figure 3.3. HOMER daily profile

3.4 PV sizing

3.4.1 PV calculation

From Table 3.1, Eq. (3.1) was used to calculate the energy consumed, where *EL* is the total energy consumption over a period, and *Ton* is the total time the load consumed power.

$$EL = load\ power\ rating\ \times Ton \tag{3.1}$$

The next step is calculating the hours during the day when the sun is most effective on the solar panel (NoH). Eq. (3.2) calculates this number, where the location irradiance is the average solar irradiance and depends on a specific location [84]. The chosen rural location's location irradiance li is 7000 Wh/m^2. This value is divided by the solar irradiance si, which is a constant of 1000 W/m^2.

$$NoH = \frac{li}{si} \qquad 3.2$$

$$= \frac{7000\,\frac{Wh}{m^2}}{1000\,\frac{W}{m^2}}$$

$$= 7\ h$$

Figure 3.4 shows the hourly average analysis of output per kW for four seasons. Different seasons generate different output power. It is noted that at 12:00, the output power is at its maximum. Power is generated from 07:00, which is sunrise, until 17 00, when sunset occurs. In summer, the sunset is around 18 00. The total number of hours that we can generate power is between 09:00 and 15: 00, which is 7 hours.

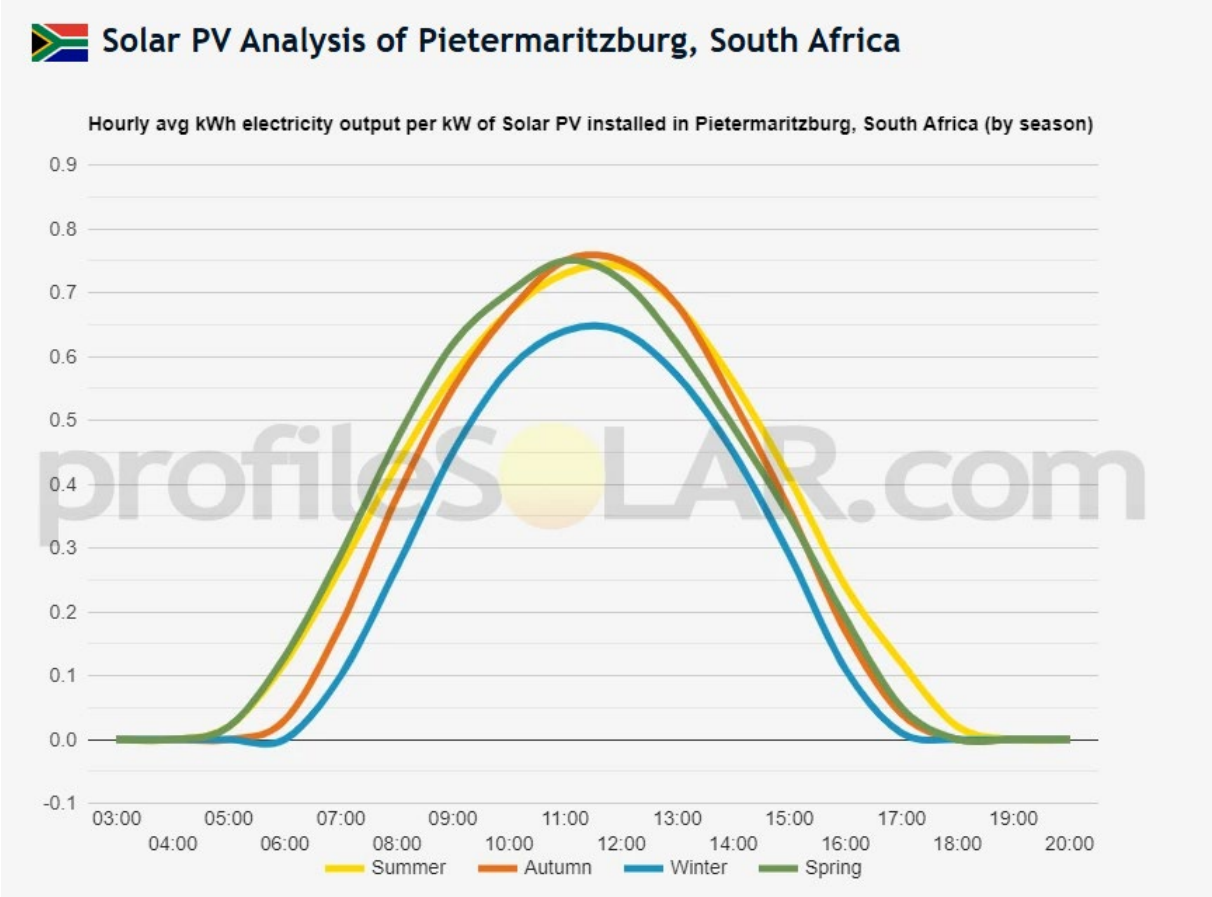

Figure 3.4: Solar PV analysis of Pietermaritzburg [85]

Eq. 3.3 where ter is the total energy required and nhm is the number of hours the sun is at maximum per day. This equation is used to obtain the solar power rating required to deliver the energy required by the loads in a day. The solar watt is the total wattage of the solar system that will supply the power to the consumers.

$$Solar\ watts = \frac{ter}{nhm} = \frac{8{,}64\ kWh}{7\ h} = 1.2\ kW \tag{3.3}$$

The solar size calculation is then compared to Figure 3.4, the HOMER software solar sizing. The calculated PV size was 1.2 kW, and the HOMER software PV size was 1 kW. The difference is caused by the number of hours the sun is at its maximum in a day. In our calculation, the number of hours was 7.

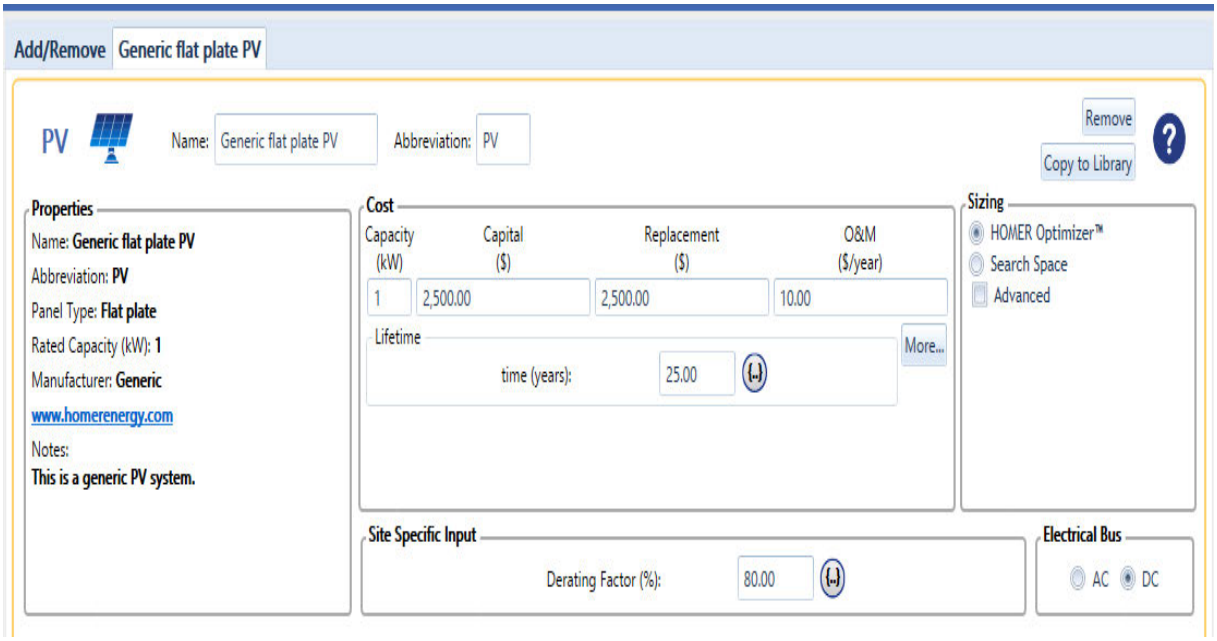

Figure 3.5. HOMER software solar sizing

3.4.2 Maximum power point algorithm selection

A converter ensured the array operated at Maximum Power Point (MPP). The voltage at which the PV module can produce maximum power is called MPP. Maximum power varies with solar

radiation, ambient temperature, and solar cell temperature. Figure 3.5 shows a graph of the current and voltage of a solar panel. The point where the product of current and voltage will be at maximum is called MPP. [86]. A Maximum Power Point Transfer (MPPT) algorithm must consistently be implemented to achieve the desired MPP.

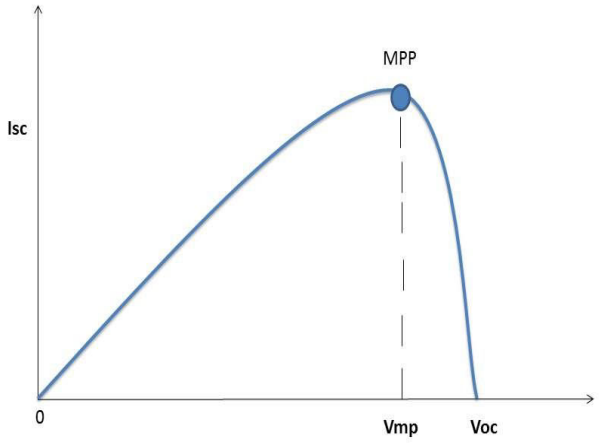

Figure 3.6. MPP of a typical solar panel

MPPT's main operation is to extract the maximum available power from solar systems by allowing it to operate at the most efficient voltage [87]. MPPT monitors the PV module's output, compares it to the previous production, and adjusts the differences in two powers to ensure that the PV operates at maximum power. MPPT is most effective under cold weather and cloudy days. In contrast, the PV module works optimally in very sunny conditions, and the MPPT is utilized to extract the maximum power available.

3.4.3 Maximum power point design

The perturb and observe (P&O) algorithm method was selected to implement a MPPT for the PV panel [88]. In this method, the previous power value is stored and compared with the most recent measured power value; the difference between the threshold and the output voltage is

then sent to control the IGBT's pulse width modulation (PWM). If the difference is a negative value as the controller increases the PWM until the value equals the threshold value to a maximum of 90%. If the difference is more significant than the threshold value, the PWM decreases until the voltage at the output equals the threshold. The PWM decreases to a minimum of 10% [89]. This method adjusts the fixed voltage, and the controller's main function is to track this value via the DC-DC converter circuits. The programming of the P&O algorithm was implemented in MATLAB® Simulink. The PWM must vary from 10% to 90%. Figure 3.6 shows the P&O algorithm flow chart. It consists of a simple feedback arrangement with current and voltage measurements. The voltage is constantly excited, and the output power is compared to the previous perturbing cycle.

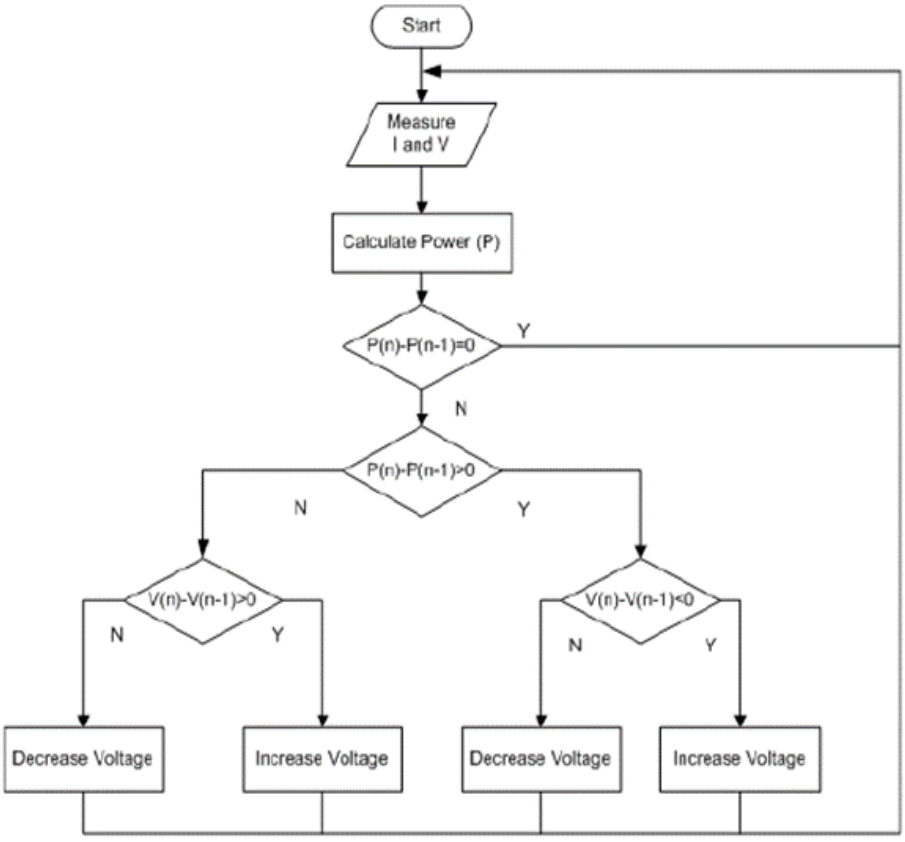

Figure 3.7. P & O algorithm flowchart

3.4.4 DC-DC converters

Figure 3.7 shows a schematic of a DC-to-DC convertor. A DC-to-DC converter is an electronic circuit that steps up or down the DC voltage [90]. Power levels range from low voltages used to power households' appliances to high voltage in power transmission. A boost converter is a DC-to-DC power converter circuit that steps up the voltage from the circuit's input to the output [68]. It is a class of switched-mode power supply (SMPS) containing at least two semiconductors, a diode, a transistor, and an energy storage element: a capacitor, inductor, or a combination thereof. To reduce ripple voltage, capacitors are added to the converter output. The power to the boost converter comes from a PV, and the PWM signal is generated by switching the insulated gate bipolar transistor (IGBT), which will be generated by the P&O algorithm to achieve the MPPT. The boost convector was chosen to meet the output voltage requirement of 48V DC as simulated in MATLAB®.

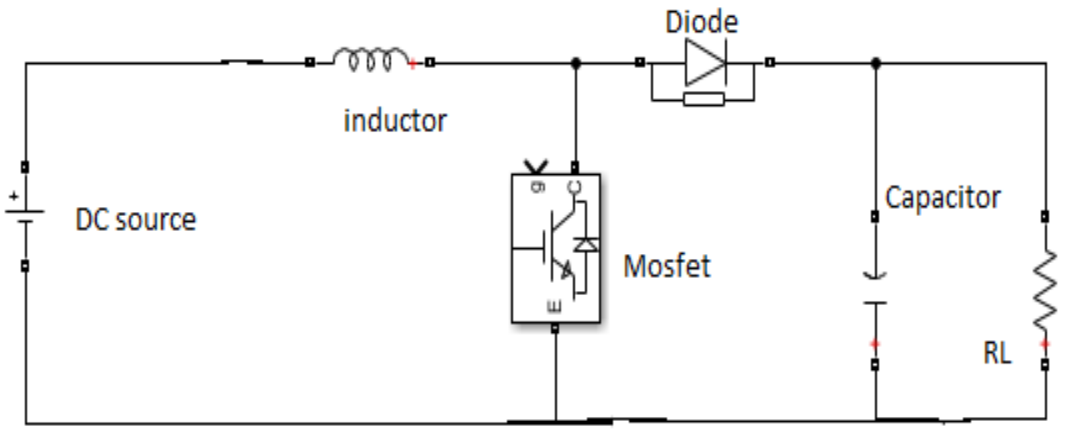

Figure 3.8. Boost converter circuit

Table 3.2 shows the boost convertor's system operating constraints. The input voltage is 29V, which is the PV rating voltage of the selected panel. The rated power is the maximum power that can be produced by the PV. The output voltage is the voltage that is required or that will be stepped up by the boost convertor. Based on the information in Table 3.2, calculations were done to size each component of the system.

Table 3.2 : Boost design specification

Specification	Value
Voltage input	29 V
Voltage output	48 V
Rated power	2 Kw
Switching frequency	50 kHz
Current ripple	5%
Voltage ripple	1%

Input Current Calculation (I_{ip}), is calculated in Eq. (3.4), where P_{in} is the input power and V_{in} is the input voltage of the boost converter.

$$I_{ip} = \frac{P_{in}}{V_{in}} = \frac{2000}{30} = 73.5\ A \quad (3.4)$$

The Ripple Current (ΔI) is calculated using Eq. (3.5). The ripple current is the current flowing to the capacitor.

$$\Delta I = 5\%\ of I_{ip} = 5\%\ 0f\ 73.5 = 3.6\ A \quad (3.5)$$

Voltage ripple calculation (ΔV) is calculated with Eq. (3.6) where V_o is the output voltage.

$$\Delta V = 1\%\ of V_o = 1\%\ 0f\ 48\ V = 0.48\ V \quad (3.6)$$

Output Current Calculation (I_{out}) is calculated in Eq. (3.7), where *P* is the power in Table 3.2, and *Vo* is the boost converter output voltage in Table 3.2.

$$I_{out} = \frac{P}{V_o} \quad (3.7)$$

$$= \frac{2000}{48}$$
$$= 42\ A$$

Inductors reduce voltage spikes that can damage the IGBTs. They also store energy when the IGBTs are closed and release this stored energy when they open. Since the frequency is very high, the value of inductance required for this purpose must be very low. To calculate the size of the inductor, Eq. 3.8 was used. L is the inductor being calculated. V input and V output are given in Table 3.2. F_{sw} is the switching frequency shown in Table 3 2.

$$L = \frac{V_{in}(V_o - V_{in})}{F_{sw} \times \Delta I \times V_o} \quad 3.8$$
$$= 6.37e^{-5}\ H$$
$$= 6.37e^{-5}\ H$$

The function of the output capacitor is to filter the current ripple and smooth the output voltage. It also must ensure that load steps at the output can be supported before the regulator can react. Capacitance calculations are calculated using Eq. (3.9). C_{out} is the output capacitor of the boost converter being calculated.

$$C_{out} = \frac{I_{out}(V_{ou} - V_{in})}{F_{sw} \times \Delta I \times \Delta V} \quad 3.9$$
$$= \frac{42(48 - 29)}{5000 \times 3.6 \times 0.48}$$
$$= 0.009\ F$$

To reduce losses, Schottky diodes should be used [91]. The forward current rating needed is equal to the maximum output current.

(i) Forward current (I_f) = average forward current of the rectifier diode.
(ii) Maximum output current I_{out} = maximum output current necessary in the application.

Schottky diodes have a much higher peak current rating than the average rating. The other parameter that must be checked is the power dissipation of the diode. It must handle:

(i) Forward current (I_f) = average forward current of the rectifier diode.
(ii) Forward voltage (V_f) = forward voltage of the rectifier diode.

IGBT is used for two purposes:

(i) For high-speed switching of the output voltage.
(ii) To provide a high current with less dissipation of heat.

The IGBT switching must resemble an ideal low-ohmic and fast switching. Switching and conduction losses must be balanced for minimum loss at the desired peak efficiency point.

3.5 Battery sizing

3.5.1 Battery calculations

After calculating the PV size, the subsequent step is to size the battery for the system and develop a BMS to monitor the charging and discharging of the battery pack. To calculate the number of batteries, the first step is to select a battery that can supply current per hour at maximum load. For this case, a battery that is rated 50 Ah is selected. When the battery rating has been selected, the following step is to decide on the depth of discharge (DOD) [92]. This is crucial as it increases the battery life span. The battery's life span is reduced when fully charged and discharged. A limit is set for charging and discharging the battery. For this calculation, a DOD of 80% is selected. The current per hour that will be drawn from the batteries under maximum load is 40 Ah, as given by Eq. (3.10).

$$80\% * 50AH = 40AH \tag{3.10}$$

The DOD calculated in Eq. (3.10) is used to calculate the energy that the battery can produce under the maximum load, as shown in Eq. (3.11):

$$\begin{aligned} energy\ required\ from\ battery &= V \times IH \\ &= 24\ X\ 40 \\ &= 0.96\ K\ Wh \end{aligned} \tag{3.11}$$

To obtain the total number of batteries required, Eq. (3.12) is used. The total system energy needed in Eq. (3.1) is divided by the energy required from the battery calculated in Eq. (3.10). From Eq. (3.12), it is seen that a total of 10 batteries will be needed. This value can be reduced by using a battery with a higher amp-hour value.

$$No.of\ batteries = \frac{solar\ energy}{energy\ required\ from\ batteries} \tag{3.12}$$
$$= \frac{8640}{960}$$
$$= 10\ battries$$

The calculated battery specification used is 24 V battery with 40 Ah and 0.96 kWh of energy needed. In the Homer software simulations, Figure 3.8 the battery was rated at 12 V with 83 Ah and 1 kWh of power needed from the battery. The lead acid was selected because of its robustness and ability to withstand harsh environment. The calculated and software generated results are similar.

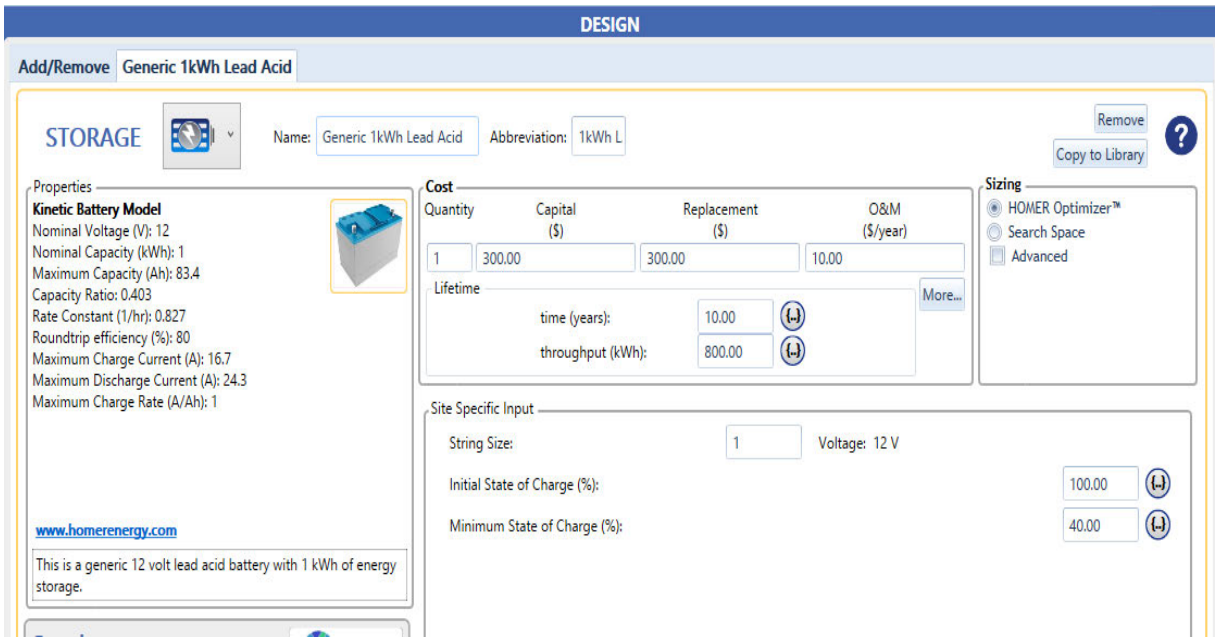

Figure 3.9. HOMER software battery sizing

3.5.2 Battery management system

BMS is a system used to monitor battery pack to ensure that batteries are operating effectively and efficiency [93]. The BMS ensures long life span of batteries and battery protection [94].

BMS provides:

i. Monitoring the battery status.
ii. Battery protection.
iii. Estimates the battery's operational state based on charging and discharging of the battery.
iv. Continually optimizing battery performance.

To implement the BMS, a bidirectional buck boost convertor is designed according to the required output voltage. Figure 3.9 shows the topology of the implemented bidirectional buck boost convertor.

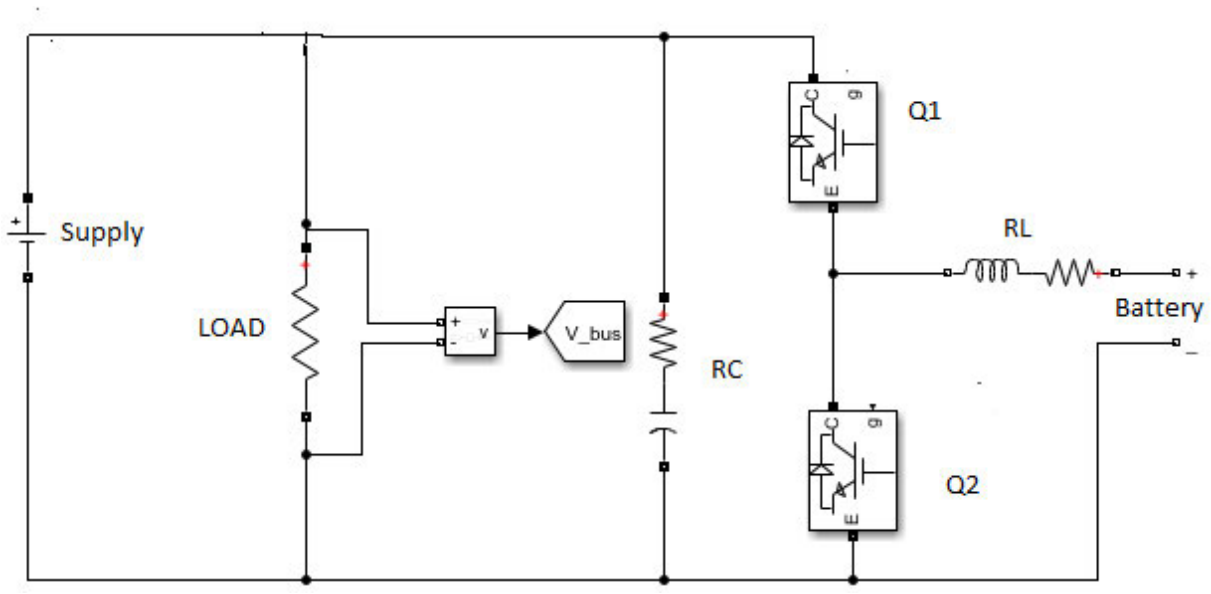

Figure 3.10. Bidirectional DC-DC buck-boost convertor

When the DC supply can produce sufficient power, the DC source will charge the battery through the bidirectional DC-DC converter and supply power to load. When the DC supply is

low, the battery will supply the load through the same bidirectional DC-DC converter and at this time, the battery discharges through load. A bidirectional DC-DC power flow converter is obtained by connecting buck and boost converter in parallel. To achieve adequate results, different PI controllers are modeled and designed to produce the desired duty cycle for MOSFET/IGBT switches [95]. The boost converter is responsible for stepping up the battery voltage to the required voltage by the load. The buck converter steps down the voltage from the solar system to the necessary voltage to charge the batteries.

3.6 Fuel cell sizing

Fuel cells convert the chemical energy of a fuel into electrical energy. The output of the fuel cell is approximately 1 kW to 10 MW. Electrical efficiency is 30% to 60% and overall efficiency is 80% to 85%. Fuel cells can use a variety of fuels, such as natural gas, propane, landfill gas, anaerobic digester gas, diesel, naphtha, methanol, and hydrogen [96]. Fuel cell systems are currently expensive energy sources in the market [97]. The two factors that contribute to this are the cost of manufacturing the fuel cell tank system and the cost of hydrogen production. Since it is expensive to operate the fuel cell at full consumer loads, it was used as a backup to supply only critical appliances, thereby reducing operating costs.

To obtain the fuel cell size needed, the first step is to study operational loads by determining the running (continuous) watts and starting (peak) watts required for each appliance. In most cases, the starting and running wattage is the same. This is the case for appliances such as TV's, lights, and laptops, whereby the starting and running wattage are the same. The starting and running wattage was the same since we focused on low-power-consuming appliances. Table 3.3 lists all appliances and wattage used to size the fuel cell.

Table 3.3 Backup load power consumption

Appliances	No of appliances	Watts
Lights	7	630
Laptops/ mobiles	7	80
Total	14	710

The total fuel cell size should be 1 kW to support all the appliances when running concurrently. The next step is to add 10% to the fuel cell size. This will allow for future appliance expansion. Therefore, the selected fuel cell size in this study is 1 kW.

3.7 Management system

3.7.1 Energy Management System

The primary function of the Energy Management System (EMS) is to increase efficiency and reduce the economic cost of operating a microgrid. EMS controls the output power generated from distributed energy resources (DERs) and gives the status of devices, forecasted load, and climate [6]. EMSs also regulate the loads' output power and energy exchanges. An EMS can be used to accomplish one or more goals, such as lowering daily operating expenses, monitoring power in real-time and reactively, minimizing losses, and balancing the energy in transmission lines [98]. In this case, an EMS is critical for microgrids to operate efficiently, ensure reliability, and satisfy short and long-term power balance. Figure 3.7 illustrates the management platform in the microgrid system proposed in this research.

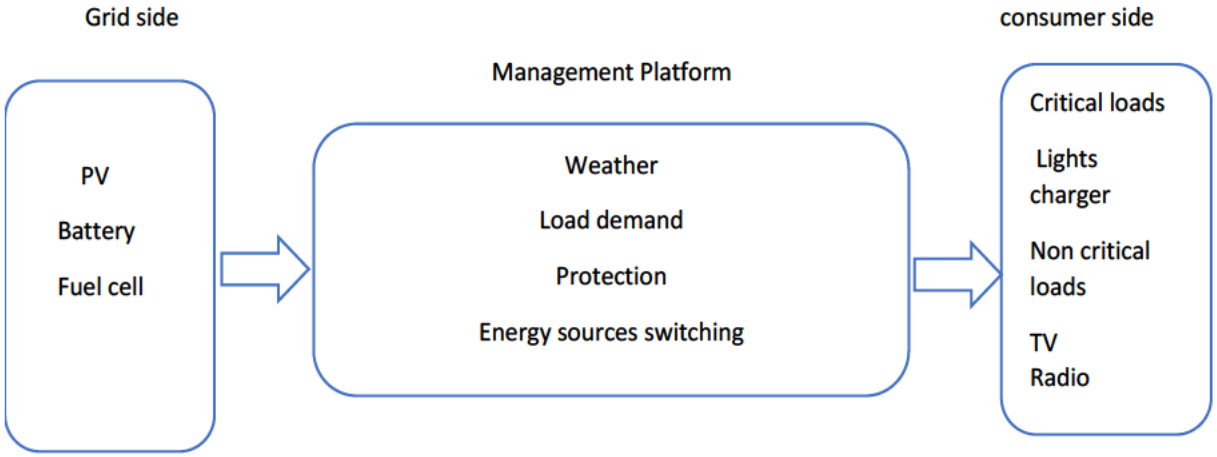

Figure 3.11. Microgrid Platform

The microgrid EMS is considered the brain of the system, and is responsible for enhancing its performance, and achieving objective functions such as isolating the loads during critical

conditions. Furthermore, EMS controls the loads in a microgrid by adequately managing the stability of the power system.

3.7.2 Demand Side Management

Demand Side Management (DSM) forms part of the EMS but focuses on the consumer side of the grid. Consumers play an essential role in microgrids as they are the users of the final product of microgrid energy. If consumers use too much energy, the grid supply can become unstable; therefore, adequate management strategies are required to specify how they operate their appliances. The development of demand-side management has been driven by the increasing demand for electricity [99].

Two DSM strategies are considered in this study. These include [99]:

i. Energy Efficiency (EE) is the decrease in energy used to provide the same quantity of goods and services. Public finances, local air pollution, overall cost, security, saving, and poverty reduction are all important energy efficiency components. Particular energy consumption, which displays the proportion of primary energy used to create a product, indicates efficiency improvement.

ii. Demand Response (DR) is the variation in electricity usage by consumers from their regular consumption trends in response to the change in electricity price over a specified time frame. DR further includes all pattern changes by end-use consumers that are proposed to alter the timing of the electricity consumers.

3.7.3 Microgrid architecture

Figure 3.11 shows the proposed microgrid architecture. The proposed architecture consists of a centralized power system placed in a specific location and powering all the properties simultaneously. This means electricity will be transported from the centralized power system to the properties or dwelling units using a wired connection. If any of the sources fail another source can take over and continue to supply power to the consumers.

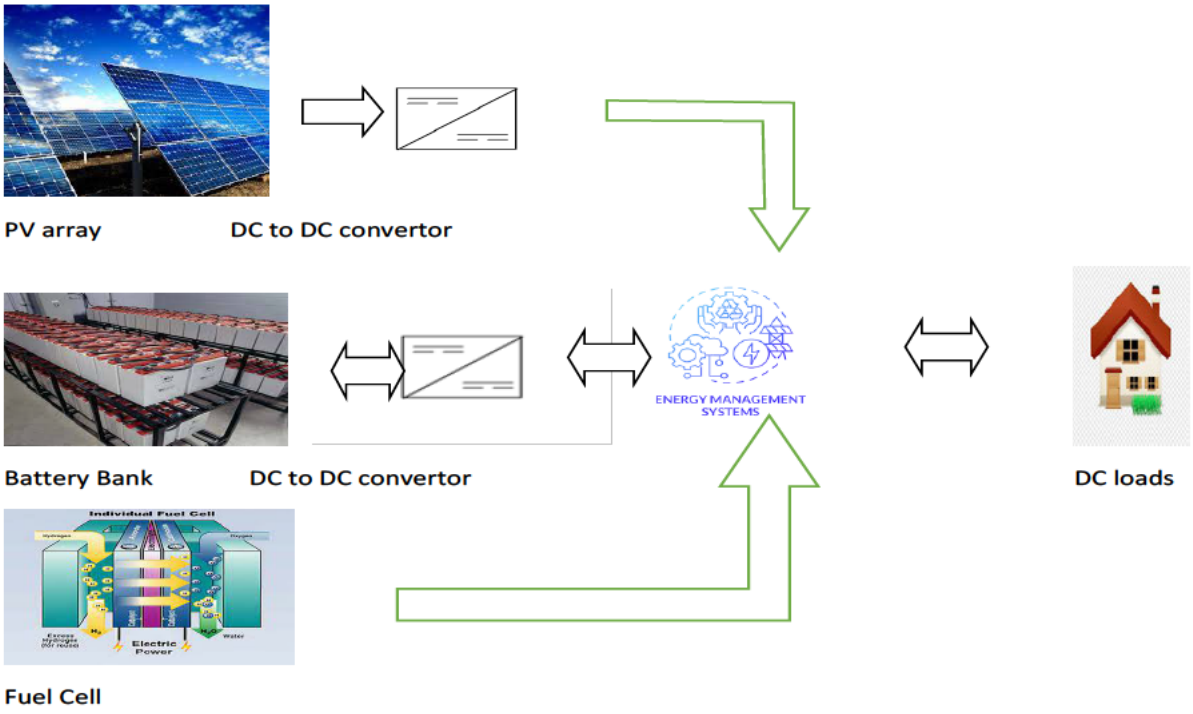

Figure 3.12: Microgrid architecture

3.8 Chapter summary

Chapter 3 focuses on the design and selection of components for the microgrid. A suitable location was selected, and the total energy consumption of the area selected was calculated. The PV, battery and fuel cell were sized based on the load consumption. After sizing the energy sources, the DC converters were chosen based on the required voltage. After the design of the converters, an energy management system was selected based on optimizing the microgrid performance.

The comparison of hand calculations with Homer software is presented in Table 3.4. The comparison looked at the energy sources which are PV and Battery. It also looked at daily profiling graphs where in the hand calculation the hourly energy usage was used to draw a graph in MALAB. In HOMER the daily profile comes automatically after entering the hourly energy usage. The solar size calculation is then compared to Figure 3.4, the HOMER software solar sizing. The calculated PV size was 1.2 kW, and the Homer software PV size was 1 kW. The

difference is caused by the number of hours the sun is at its maximum in a day. In our calculation, the number of hours was 5. The calculated battery specification used is 24 V battery with 40 Ah and 0.96 kWh of energy needed. In the Homer software simulations, figure 3.8 the battery was rated at 12 V with 83 Ah and 1 kWh of power needed from the battery. The calculated and simulated results are almost the same.

Table 3.4*:* Comparison between Hand Calculated and HOMER software

	Human Calculated results	Homer software results
PV sizing	1,2 kW	1 kW
Battery sizing	0.96kWh	1kWh
Battery voltage	24V	12V
Battery Current	40Ah	83,4Ah
Daily profiling	MATLAB drawn with data	Automated based on given data
Cost	No cost provided	Provides total cost

Chapter 4 System Modelling and Simulation

4.1 Introduction

Chapter 4 presents the modelling and the simulation of the solar cell, boost convertor, bidirectional system based, fuel cell and an energy management system based on the calculations in the prevoius chapter. Detailed descriptions of developed MATLAB® Simulink models is given.

4.2 Solar cell modelling

Figure 2.3 showed the equivalence of a single solar cell circuit. From figure 2.3 , equations can be derived and these equations can be used to model the solar cell in the simulation environment. Solar cells generate an internal current proportional to the light intensity. Not all this current is available to the load because some flow through the parallel diode and some flow through the shunt resistor. When no load resistance is present, the voltage available at the terminals of the solar cell is determined by the interaction of the current source with the parallel diode and the parallel resistance. This is called the open-circuit voltage. If the cell supplies load is current, the voltage at the terminals will be lower than the open-circuit voltage because some of the voltage is dropped across the series resistance.

Table 4.1 gives the specification of a PV panel that was selected for the MATLAB™ simulation. The PV panel was selected based on calculations in PV sizing in Chapter 3. These parameters were then used to model the PV and simulated, and the result was compared with thhe built in PV in MATLAB™ .

Table 4.1. Solar cell specification

Specification	Values
Voltage at maximum power (Vmp)	29V
Current at Maximum power (Imp)	8.2A
Open circuit voltage(Voc)	36V
Short circuit current(Isc)	5A
Total number of cells in series(Ns)	10
Rated power	231
Total number of cells in parallel(Np)	1

There are 5 equations that can be derived from figure 2.3, the first equation is Reverse saturation current I_{rs} is the part of the reverse current in a semiconductor diode caused by the diffusion of minority carriers from the neutral regions to the depletion region. The equation to obtain the reverse saturation is shown in Eq. (4.1) and appendix B is MATLAB™ equavelent equation. In Eq. (4.1) I_{rs} is the reverse saturation that is being modelled, where I_{sc} is the short circuit current, q is the electronic charge, Voc is the open circuit voltage, n is the ideal fector of the diode, Ns is the number of cells connected in series, J is the boltzman constant which is 1.38×10^{-23}, and T is the operating temperature in Kelvins.

$$I_{rs} = \frac{I_{sc}}{e^{\left(\frac{q*V_{oc}}{n.N_s*J*T)}\right.} - 1} \tag{4.1}$$

Saturation current variables in Eq. (4.2), include I_o which is the saturation current, T_n is the nominal temperature, and E_{go} is the band gap of the semiconductor. The MATLAB™ model of the saturation current is presented in appendix C.

$$I_o = I_{rs} * \left(\frac{T}{T_n}\right)^3 * exp^{\left[\frac{q*E_{go}*\left(\frac{1}{T_n}-\frac{1}{T}\right)}{n*J}\right]} \tag{4.1}$$

I_{ph} is the electric current through a photosensitive device, such as a photodiode due to exposure to radiant power. The photocurrent may occur because of the photoelectric, photo emissive, or photovoltaic effect. G is solar irradiation.

$$I_{ph} = [I_{sc} + k_i(T - 298)] * \frac{G}{1000} \tag{4.2}$$

To model the current through shunt resistor (I_{sh}) as shown in Eq. (4.4) the shunt resistance (R_{sh}) and series resistance (R_s) is used. It should be noted that during normal operation, the efficiency of solar cells is reduced by the dissipation of power across internal resistances.

$$I_{sh} = \frac{V + I * R_s}{R_{sh}} \quad 4.3$$

Finally, the output current combines Eq. (4.1) and Eq (4.4), to yield the output current as shown in Eq (4.5).

$$I = I_{ph} - I_o * \left[e^{\left(\frac{q*(V+I*R_s)}{n*J*N_s*T}\right)} - 1 \right] - I_{sh} \quad 4.4$$

Appendix F is a complete model of solar cells. Appendix H illustrates the model when the solar cell is simulated using two scopes to plot power versus current and voltage versus current in time domain.

4.3 Boost convertor mathematical modelling and analysis.

A mathematical model was obtained for the boost converter circuit based on theory of its working principle. Mathematical modeling is defined by the capacitor and inductor in the boost converter. Inductor voltage and capacitor current are given in Eq. (4.6) and Eq. (4.7), respectively.

4.3.1 Equation modelling

Eq. (4.6) and Eq. (4.7) were used to model the boost converter in Eq. (4.6). V_L is the voltage across the inductor and L is the inductance, which is being derived with change in time. In Eq. (4.7), I_C is the current flowing through the capacitor (C).

$$V_L = L\frac{di_L}{dt} \quad 4.5$$

$$I_c = C\frac{dv_c}{dt} \quad 4.6$$

Using Kirchhoff Current Law (KCL) in Figure 4.2 and Figure 4.3, we derive two equations. V_{in} is the DC source as shown in Figure 4.10 and Figure 4.11.

$$L\frac{di_L}{dt} = V_{in} \quad 4.7$$

$$C\frac{dvc}{dt} = -\frac{Vc}{R} \quad 4.8$$

While inductor voltage V_L is used for PWM switching conditions are given in Eq. (4.10) and Eq. (4.11) respectively.

$$V_L = V_{in} * PWM \quad 4.9$$

$$V_L = (V_{in} - V_{out}) * \overline{PwM} \quad 4.10$$

The switching times are determined by the PWM switching frequency and its duty cycle.

$$PWM = \frac{(V_{out} - V_{in})}{V_{out}} {f_{PWM}}^{-1} \quad 4.11$$

The current flowing through can be determined by integrating Eq. (4.13).

$$I_l = \frac{1}{L}\int V_L dt \quad 4.12$$

After obtaining the current through the inductor, the current through the capacitor can be determined in Eq. (4.14), where I_R is the current through load resistor.

$$I_c = I_L - I_R \quad 4.13$$

Thereafter the capacitor voltage can be calculated from Eq. (4.15), which indicates the load voltage of the boost converter in the case of the ideal model.

$$V_c = \frac{1}{C}\int I_C dt \quad 4.14$$

Figure 4.1 is a complete model of a boost converter derived from the equations previously described. The respective inductor and capacitor values were calculated based on the system ratings from Table 3.2.

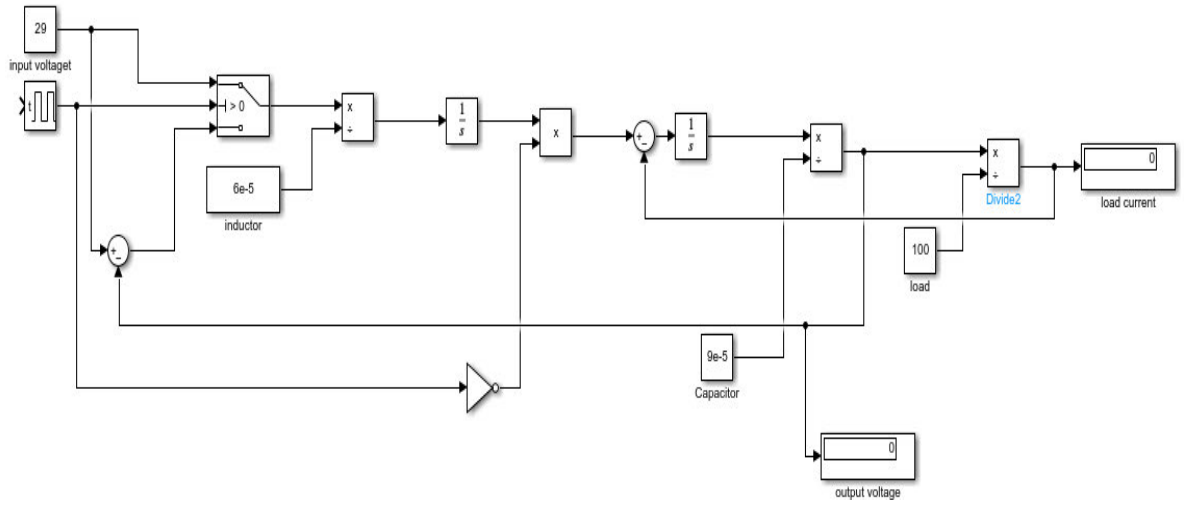

Figure 4.1 Boost convertor simulation model

4.3.2 State space modelling

When the system is in open loop mode (switch open), the inductor release energy and the capacitor stores energy.

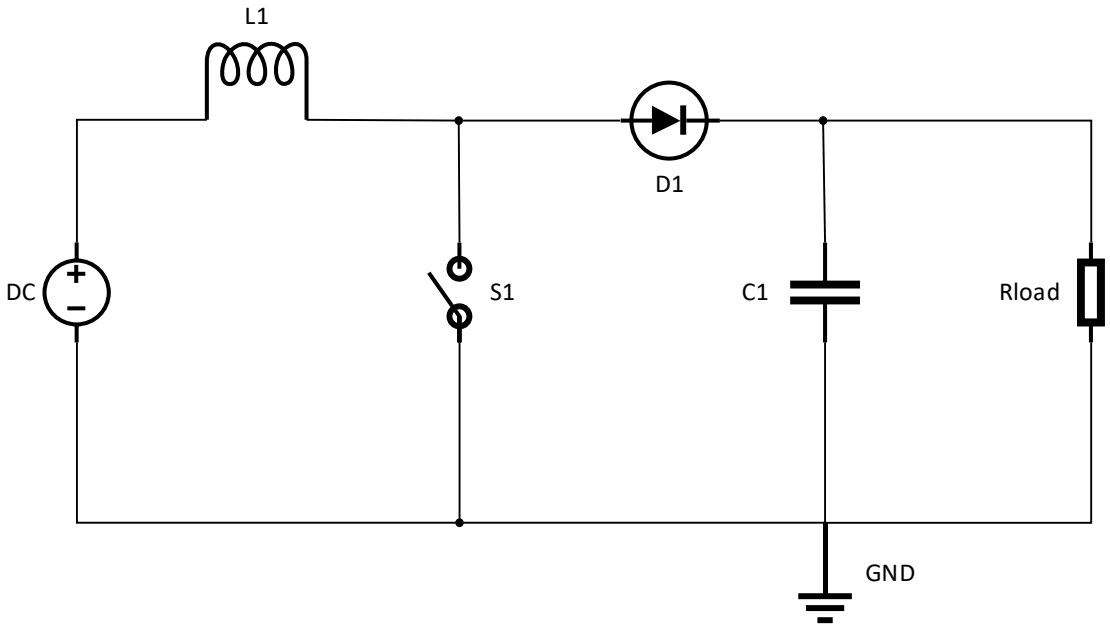

Figure 4.2 . Boost convertor open mode circuit

From this circuit, using KCL analysis when the switch is open, we obtain:

$$L\frac{diL}{dt} = Vin - Vc \tag{4.15}$$

$$C\frac{dvc}{dt} = I_L - \frac{Vc}{R} \tag{4.16}$$

Where,

$I_L = I_{in}$= the current flowing through the inductor.

$V_c = V_{out}$ = the voltage across the capacitor.

Let the state variables be defined as:

$$x_1 = I_L \tag{4.17}$$

$$x_2 = V_c \tag{4.18}$$

$$\begin{bmatrix} \dot{x}_1 \\ \dot{x}_2 \end{bmatrix} = \begin{bmatrix} 0 & \frac{-1}{L} \\ \frac{1}{C} & -\frac{1}{RC} \end{bmatrix} \begin{bmatrix} X_1 \\ X_2 \end{bmatrix} + \begin{bmatrix} \frac{1}{L} \\ 0 \end{bmatrix} V_{in} \tag{4.19}$$

Similarly in closed loop, the inductor stores energy and the capacitor releases energy.

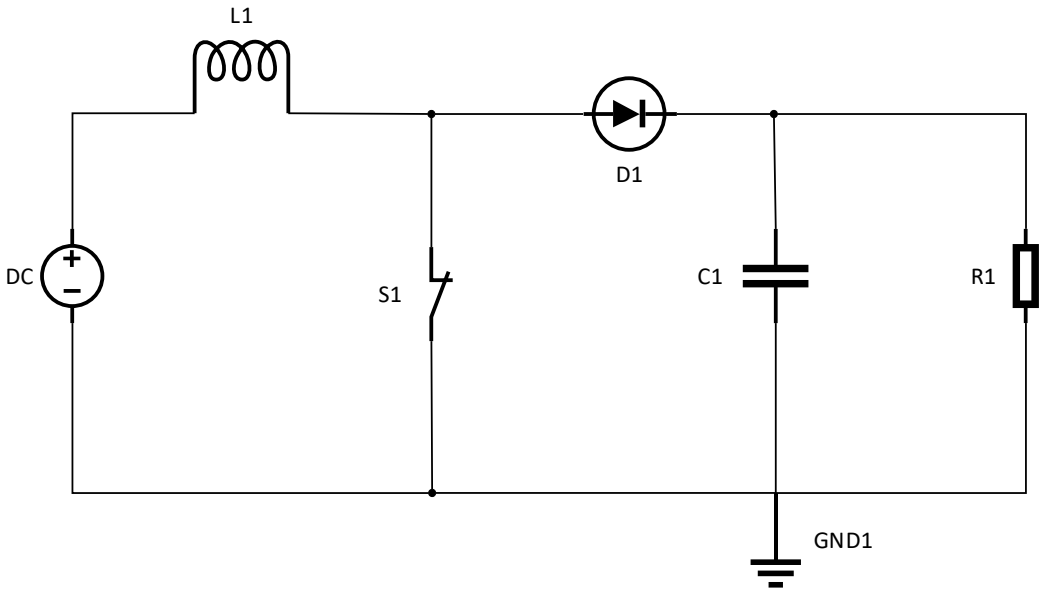

Figure 4.3. Boost convertor closed mode model.

This is modeled as:

$I_L = I_{in}$ = the current of inductor.

$V_c = V_{out}$ = the voltage of capacitor.

The state variables are then defined as:

$$x_1 = I_L;\ x_2 = \text{Vc}$$

The output equation is then assigned the state variables, where:

$$\begin{bmatrix} \dot{x}_1 \\ \dot{x}_2 \end{bmatrix} = \begin{bmatrix} 0 & 0 \\ 0 & -\frac{1}{RC} \end{bmatrix} \begin{bmatrix} X_1 \\ X_2 \end{bmatrix} + \begin{bmatrix} \frac{1}{L} \\ 0 \end{bmatrix} V_{in} \qquad 4.20$$

Combining the state space equations, Eq. (4.20) and Eq. (4.21), results in Eq. (4.22) by the averaging method:

$$\dot{x} = \bar{A}\boldsymbol{x} + \dot{B}\boldsymbol{u} \quad (4.21)$$

Where, $\bar{A} = A_1 d + A_2(1- d)$

and $\dot{B} = B_1 d + B_2(1 - d)$

$$\dot{x} = \begin{bmatrix} 0 & \frac{-(1-d)}{L} \\ \frac{1-d}{C} & -\frac{1}{RC} \end{bmatrix} x + \begin{bmatrix} \frac{1}{L} \\ 0 \end{bmatrix} V_{in} \quad (4.22)$$

$$Y = [0 \quad 1] * \begin{bmatrix} i_l(t) \\ V_c(t) \end{bmatrix} + [0]V_{in} \quad (4.23)$$

4.3.3 Transfer function

The Boost converter is modelled in the Laplace domain using transfer function modeling techniques. From Figure 4.11, the total impedance of the boost converter when switch is OFF is given by:

$$Z_{total}(S) = Z_1(S) + Z_2(S) \quad (4.24)$$

And Z_1 is given by:

$$Z_1(S) = \frac{Vin(S)}{I(S)} = Z_{parallel} + Ls \quad (4.25)$$

$Z_{parallel}$ is given by:

$$\frac{1}{Z_{parallel}} = \frac{1}{R} + \frac{1}{\frac{1}{Cs}} \quad 4.26$$

Simplifying Eq. (4.27) we obtain:

$$\frac{1}{Z_{parallel}} = \frac{1}{R} + Cs \quad 4.27$$

$Z_{parallel}$ is defined as:

$$Z_{parallel} = \frac{R}{1 + RCs} \quad 4.28$$

Therefore, Z_1 is given by:

$$\frac{Vin(S)}{I(S)} = \frac{R}{1 + RCs} + Ls \quad 4.29$$

$$\frac{Vin(S)}{I(S)} = \frac{RCLs^2 + Ls + R}{RCs + 1} \quad 4.30$$

Solving for Z_1 to get V_{in} as the subject of the formula we derive:

$$Vin(s) = \frac{RCLs^2 + Ls + R}{RCs + 1} * I(s) \quad 4.32$$

$Z_2(s)$ is given by:

$$Z_2 = \frac{Vo(s)}{I(s)} = Z_{parallel} = \frac{R}{1 + RCs} \quad 4.31$$

Making $V_o(s)$ subject of the formula from Eq. (4.33) we obtain:

$$Vo(s) = \frac{R}{RCs + 1} * I(s) \quad 4.32$$

Therefore, the transfer function is given by Eq. (4.34):

$$\frac{Vo}{Vin} = \frac{R}{RCLs^2 + Ls + R} \quad 4.33$$

4.4 Solar with boost convertor and MPPT

After the mathematical modelling of the solar and boost converter, a PV system with a boost converter was then defined and modelled. Figure 4.4 shows the model of the PV with boost converter. To achieve the desired 2kW rating a parallel connection of ten panels were used. A boost converter was used to implement an MPPT P&O algorithm as simulated in the MATLAB™ environment.

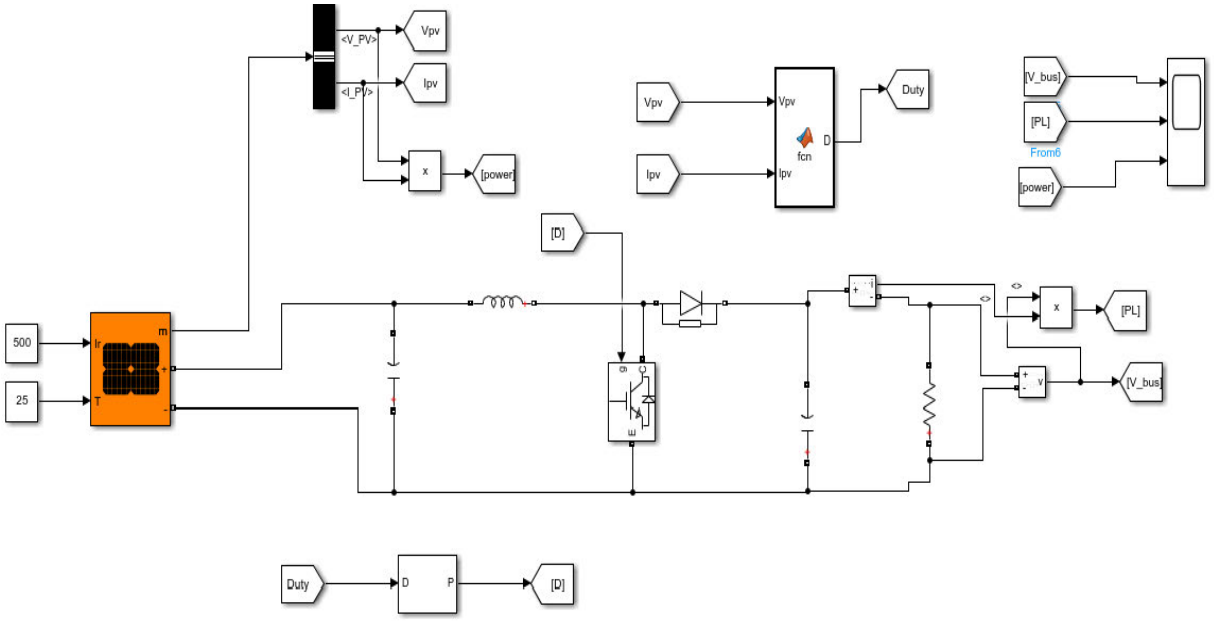

Figure 4.4. MPPT model with PV

4.5 Battery charging and discharging modelling.

After modelling the boost converter, the next stage was to model the complementary battery charging system using the design parameters as previously described. Figure 4.5 shows the model of the battery charging and discharging circuit. A PI controller was developed to control the charging and the discharging of the battery. The bidirectional buck-boost converter circuitry affects the charging and discharging of the battery. The buck circuit is used to step down the voltage to 24V from 48V such that the battery can be charged. When the battery is full, the boost converter is used to step up the 24V to 48V to supply the load.

If the supply source is offline, the battery is the main source of power for the load. Once restored, the supply is directed to the load and subsequently charges the battery.

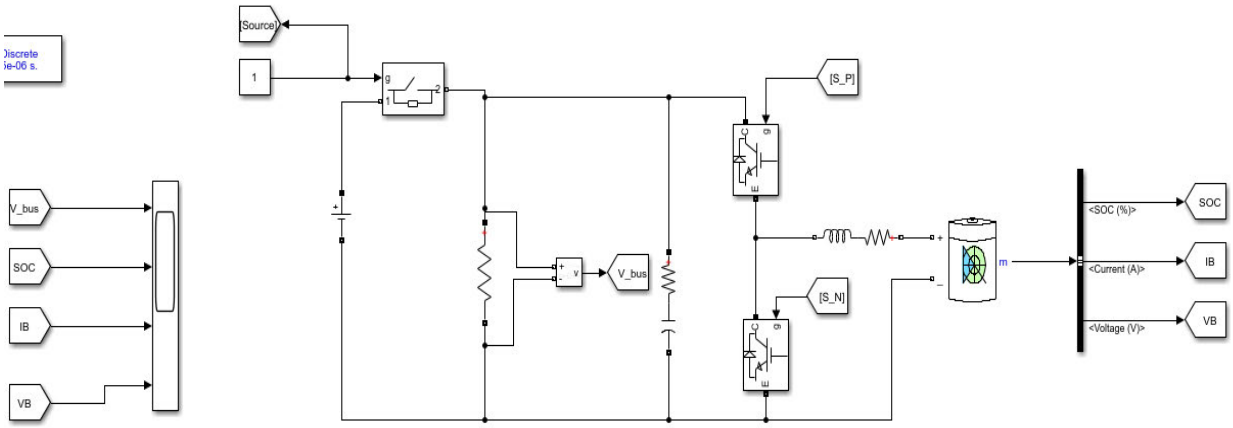

Figure 4.5. Batter charging and discharging model.

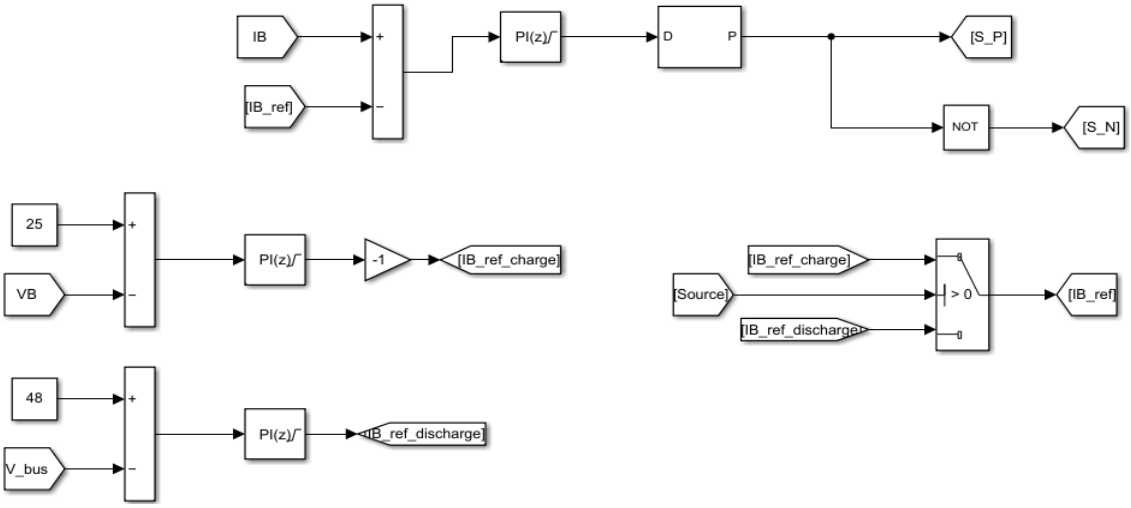

Figure 4.6. Battery control system

4.6 Fuel cell modelling

The fuel cell was modelled and shown in Figure 4.7. It illustrates the modelled fuel cell connected to the boost converter. The boost convertor increases the 24V from the fuel cell to 48V across the load.

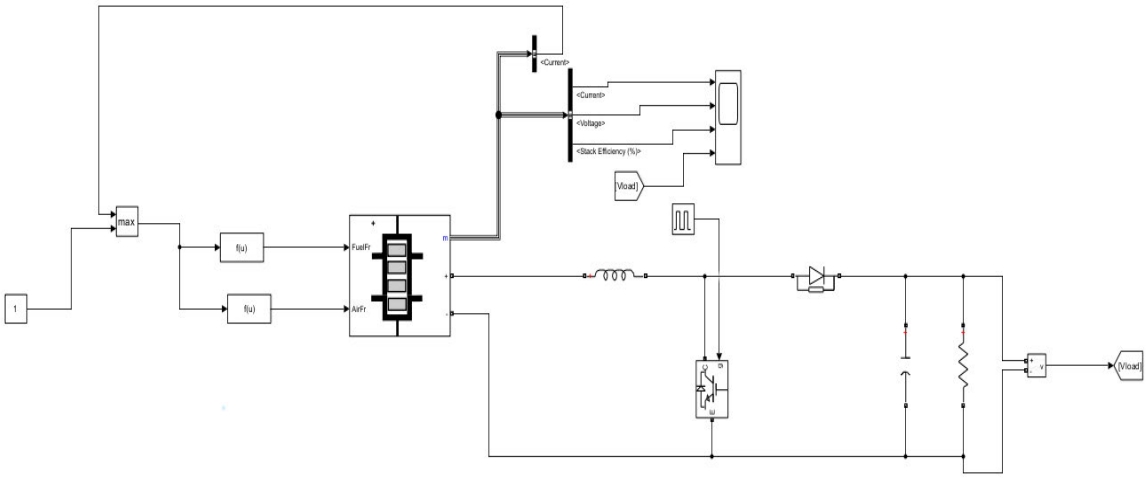

Figure 4.7. Fuel cell model

4.7 Complete model

Figure 4.8 shows the MATLAB™ simulation of the microgrid with three separately controlled sources. The first source was the PV which is connected to the load by a boost convert. The boost convert was used to boost the 29V from the PV to 48V which was required by the load. A MATLAB™ function was created which contained a P&O MPPT algorithm. This algorithm ensures maximum power availability from the PV.

The second source was the battery for which there is a complementary bidirectional buck- boost converter. The buck part is used to step down the PV voltage from 48V to 24V which is required to charge the batteries. The 24V from the battery is boosted up to 48V DC to supply the load. At that time, the PV is disconnected from the grid. When the battery has discharged, the PV is still not generating any power. The fuel cell starts supplying the load, at which time the battery is disconnected, and critical loads are supplied. The energy management system selects which energy source is going to be used based on the energy demand, availability of the sun and finally the state of charge of the battery. The three components were independently controlled, and a switching algorithm was created using a MATLAB™ function. This was implemented to safeguard the microgrid in case of failure of one or two components, allowing the remaining components to continuously supply the load, especially during unexpected faults or planned maintenance.

During peak load periods, the microgrid utilized a direct load control program. This type of demand response program is utilized to cut off non-essential loads through a controlled switch. This strategy is employed when energy usage is high, and the PV system is unable to generate sufficient power due to the absence of sunlight and while the batteries may have insufficient charge to support the consumers. By directly controlling the loads, the microgrid can shut down the entire demand side using the load clipping method, which allows for selective control of non-critical loads based on their operational characteristics.

The loads were categorized into critical and non-critical loads. Critical loads are those whose operation cannot be interrupted, such as security lights at night, while non-critical loads are those that can be interrupted for a certain period, for example, televisions. In conditions of high demand, load clipping is applied to non-critical appliances, ensuring that only critical appliances receive power. In these situations, the fuel cell is employed as the third energy source to exclusively supply the essential loads. When power is available from one of the first two sources, the fuel cell is deactivated, allowing the PV system or battery to supply the consumers.

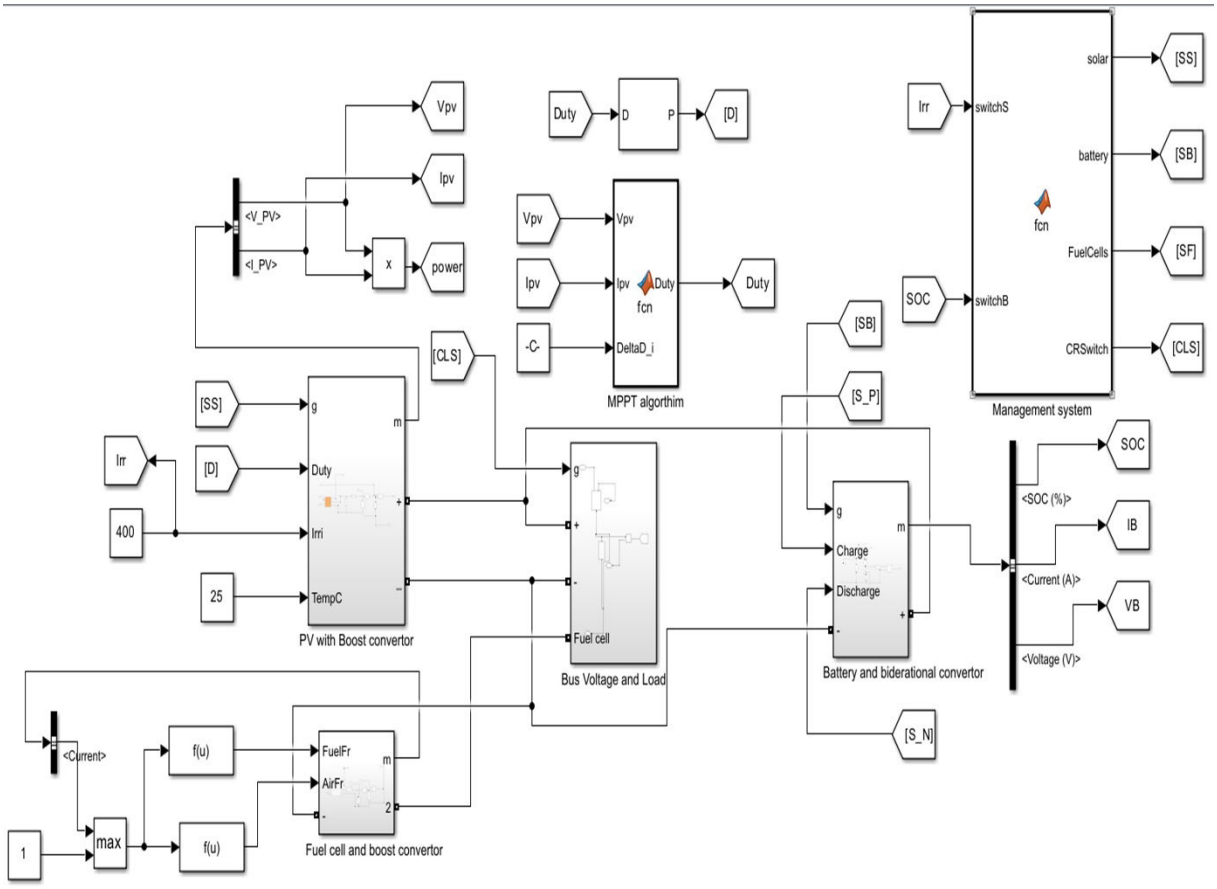

Figure 4.8. PV, battery, and fuel cell optimization model

4.8 Chapter summary

This chapter focuses on the modelling and simulation of the proposed microgrid. A mathematical model was described for a solar cell with the aim of extracting the MPPT of the system. The buck and boost circuitry for managing the batteries was explained. A fuel cell model was developed and incorporated into the overall model. Finally, energy management was modelled and simulated to manage the complete model.

Chapter 5 Results and Discussion

5.1 Introduction

This chapter presents the model simulation results from the systems described in Chapter 4. An analysis of each experiment is provided.

5.2 Solar Cell simulation results

Figure 5.1 shows the PV simulation results. The output is derived from the PV array block parameter with specifications as shown in Table 4.1. The first graph shows the current versus voltage with the temperature at 25 °C. The second graph was for the power versus voltage. It was observed that the maximum power point that the PV can produce was 200W at ±29V DC. This is the MPPT of the PV with a maximum current of 8A.

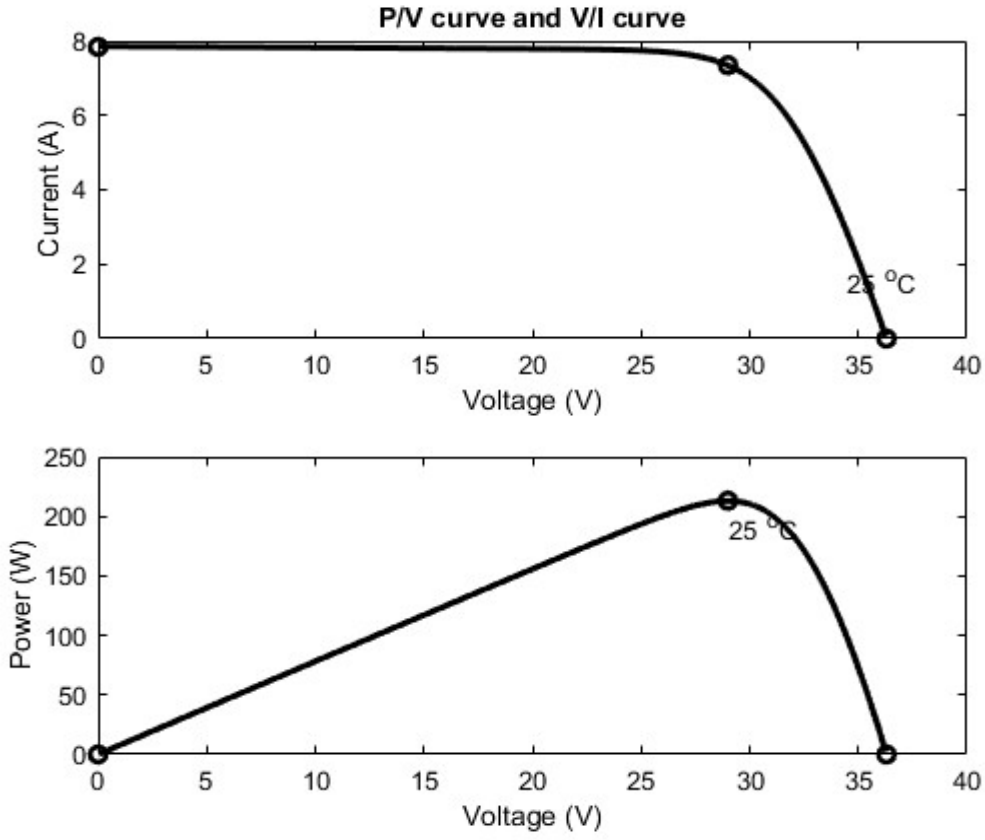

Figure.5.1. Simulation of PV power and voltage model

In Figure 5.2, the P/V curve is compared to results of Figure 5.1. At voltage ±28V the power consumption was approximately 200W and at 28V the power decreased substantially. Therefore, the maximum power that that the PV can produce is 200W at 28V. This value is the same as the value that was obtained when simulated the PV block parameter. The irradiance was set at 1000m^2.

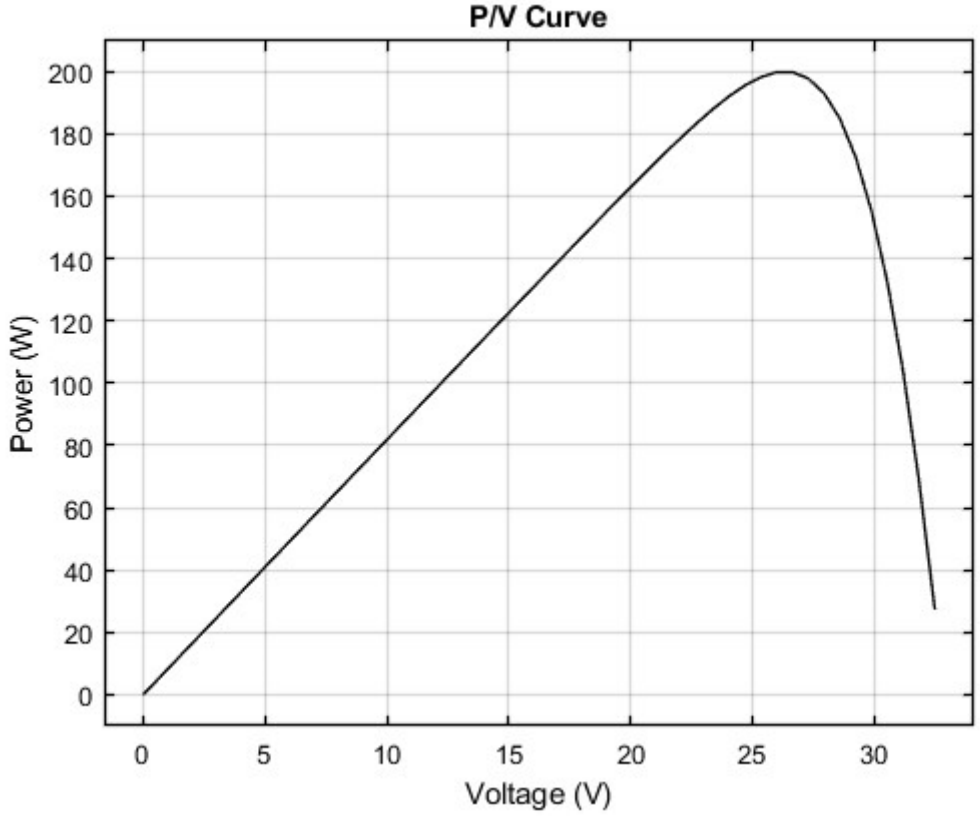

Figure 5.2. Model solar cell power graph

Figure 5.3 shows the simulation results for the current versus voltage for the solar cell. The current was above 8A, the solar cell model was set at 25°C and 1000m^2 irradiance. The result was compared to Figure 5.1 V/I curve. In Figure 5.1, the current was at 8A and there is a negligible difference between the PV block parameter and mathematical modelled PV.

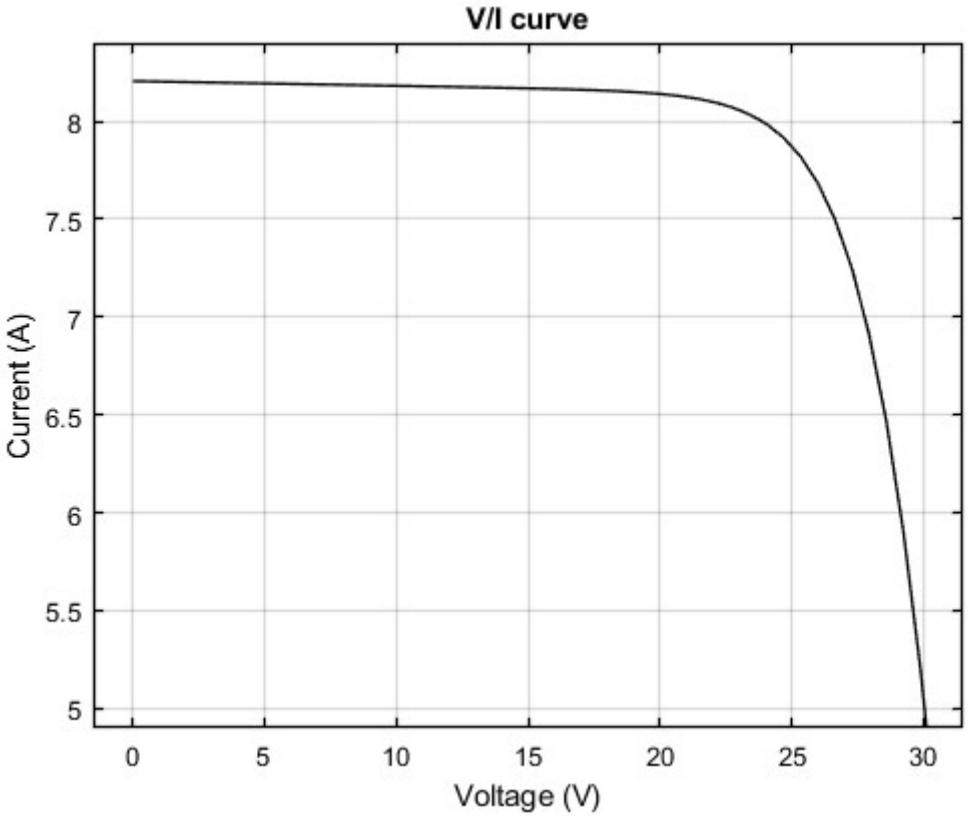

Figure 5.3. Modelled solar cell current output.

The mathematical modelling of a solar cell was verified as the results were similar to the MATLAB™ PV block parameters.

5.3 Solar MPPT simulation results

Figure 5.4 shows the simulation results of a PV MPPT with a boost converter. The main objective was to extract maximum power across the load that is at the input of the PV. Annexure A shows the MPPT algorithm code used to obtain the results. The x-axis is shown in terms of time in hours (hrs). As the irradiance varied from sunrise to sunset, the output power was observed. When the irradiance was increased, the PV harvested more energy for which the load was able to extract the maximum power available from the system. Suffice to say, when the irradiance was decreased to the minimum value, the PV harvested less energy. The power at the input of the PV was equal to the power at the load side.

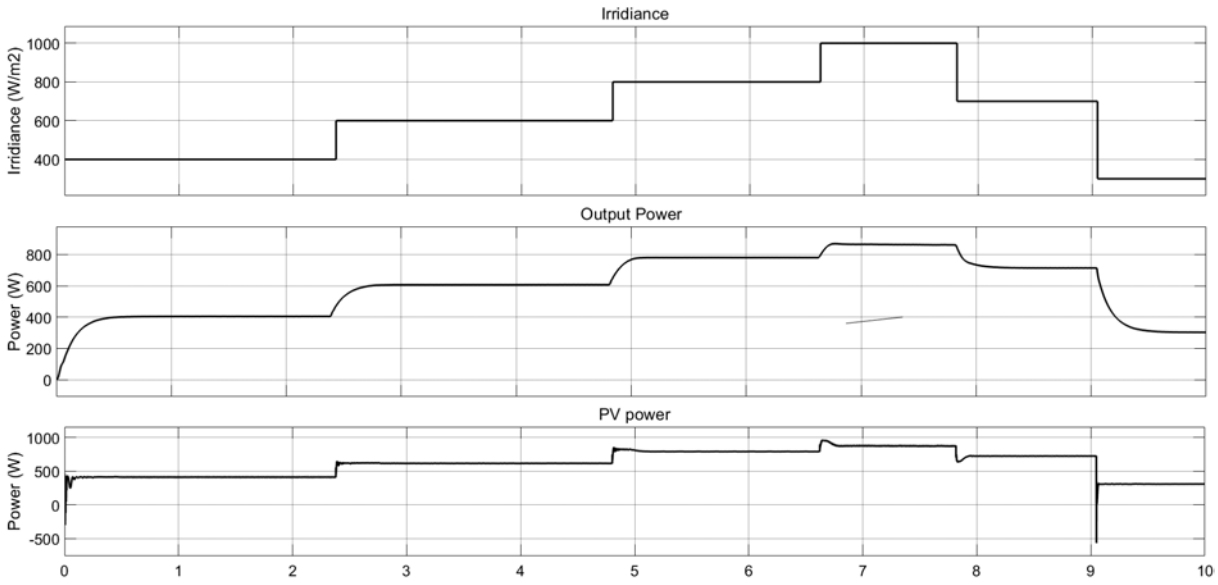

Figure 5.4. MPPT simulation results

The irradiance varied from 0 to 1000W/m^2. The initial value of the irradiance was set at 400W/m^2. The power produced by the PV was 400W and which also resulted in an overall system output of 400W. When the irradiance was increased at T = 2.4hrs to 600W/m^2, the output power increased proportional to the PV power. This implied the at any given stage, the power at the output was the same as the power produced which suggested that the MPPT circuit simulation functioned as expected.

5.4 Battery Simulation Results

Figure 5.5 shows the battery simulation results as given by the block diagram in Figure 4.5. The switching was done between the 48V DC source and the battery. When the switch was at the 'high position', the voltage source was charging the battery and supplying the load with power. The bus voltage was at ±48V throughout the simulation. The battery state of charge increased when the switch was high to show charging of the battery and correspondingly decreased when discharging as the switch was changed to the 'low position' as the battery was being drained by the load. A battery current with a negative value indicates charging and a positive value shows the discharging of the battery with a 24V voltage. At T = 6hrs the switch was turned 'off' and it was observed that the battery started discharging by supplying power to the loads.

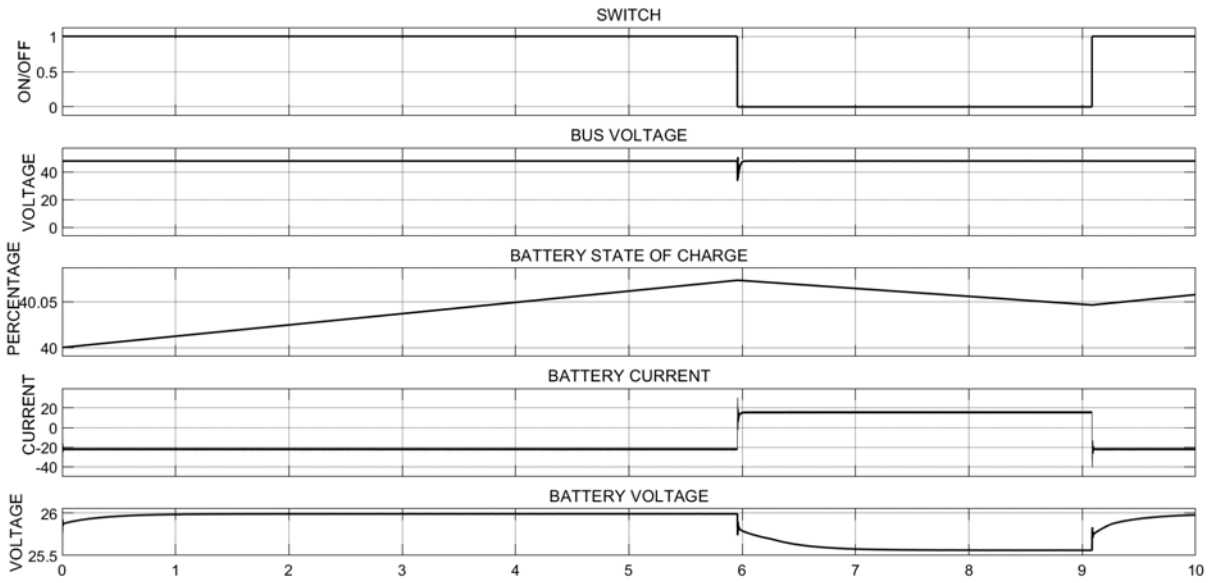

Figure 5.5. Battery charging and discharging simulation

The sharing of power between two sources is crucial as it ensures constant energy supply to the load for system redundancy. From charging the battery and supplying the load with 48V DC, the function of bidirectional buck boost convert is also observed as the battery voltage is observed at ±26 V. This implies that the buck part of the bidirectional converter was stepping down the 48V to the batteries required voltage for the sake of charging. When the switch was at 'low' position, the battery supplies the load with stable power due to the bidirectional convertor circuitry.

5.5 Fuel cell results

Figure 5.6 shows the results obtained from the fuel cell modeling simulation. The fuel cell's output current being drawn by the load was ±22A at a corresponding voltage ±34V. With a 40% efficiency of the fuel cell a boost convert was used to achieve the desired 48V across the load which can be observed in DC bus voltage trend.

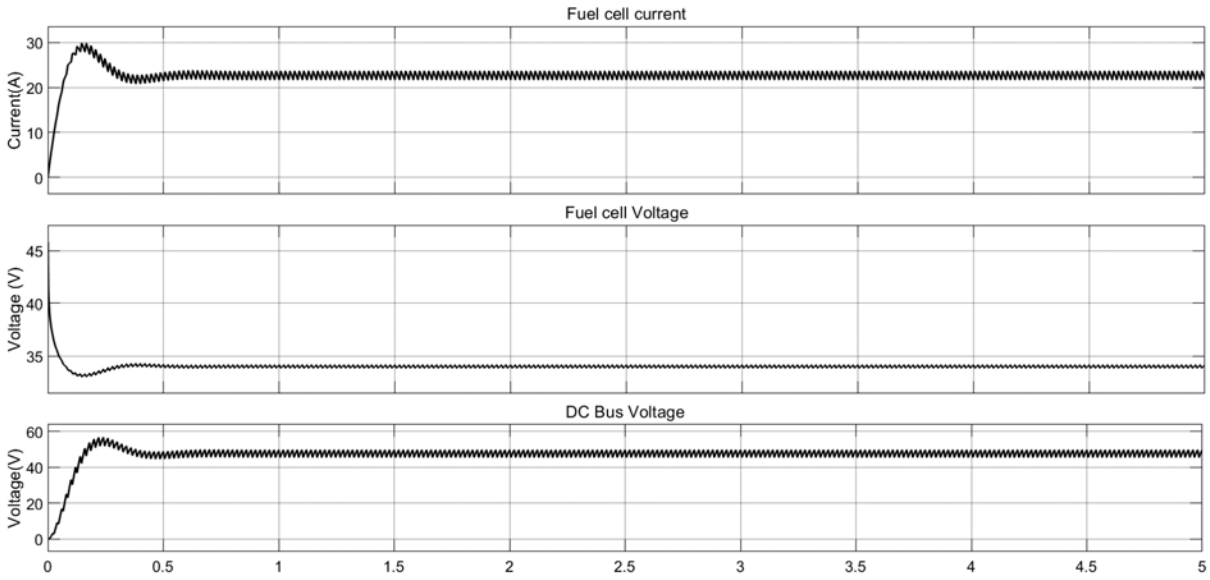

Figure 5.6. Fuel cell simulation results

5.6 Complete system simulation results

In Figure 5.7, the overall model's results are displayed without load clipping. It is evident that the bus voltage is maintained at ±48V DC with a noticeable disruption at T = 6hrs and at T = 15hrs when a transition occurs due to supply source changeover. During the simulation period T = 0hrs to T = 6hrs, PV system was supplying power to the load while charging the battery. The irradiance levels were increased from 500W/m^2 to a maximum of 1000W/m^2 with a relatively stable power of 400W being output to the load. This scenario is typical of the period from sunrise to midday when the sun is ascending to its peak, allowing the PV array to produce power at its maximum rated level. Consequently, the battery's state of charge marginally increased as it was being charged. At T = 3hrs, the irradiance decreased to 700W/m^2, which impacted the battery's rate of charging. When the irradiance decreased to 400W/m^2 at T = 6hrs, the PV system was automatically disconnected from the microgrid by the PV isolation switch. Subsequently, the battery started supplying the system load thereby resulting in the battery's discharge. At T = 15hrs, the fuel cell began supplying power to the load and maintained an output ±400W. It should be noted that the fuel cell was responsible for supplying both critical and non-critical loads. The next simulation results describe the system with load clipping when the fuel cell is under use.

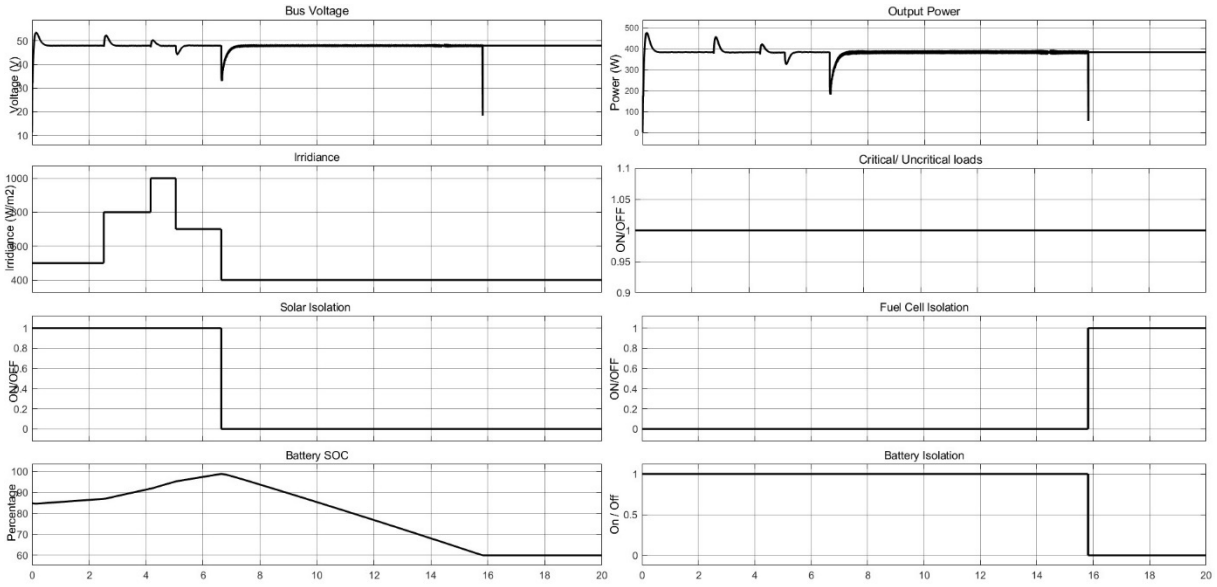

Figure 5.7. Complete model results without load clipping

In this scenario, when the fuel cell is supplying power, load clipping is applied to ensure that only critical appliances are powered. Figure 5.8 depicts the impact of load clipping on the microgrid. At T = 15hrs, when the fuel cell starts, the uncritical loads are disconnected, increasing output power from 400W to 780W indicating minimal strain on the fuel cell and reduced hydrogen consumption. Thereby extending the longevity of the fuel cell's hydrogen consumption.

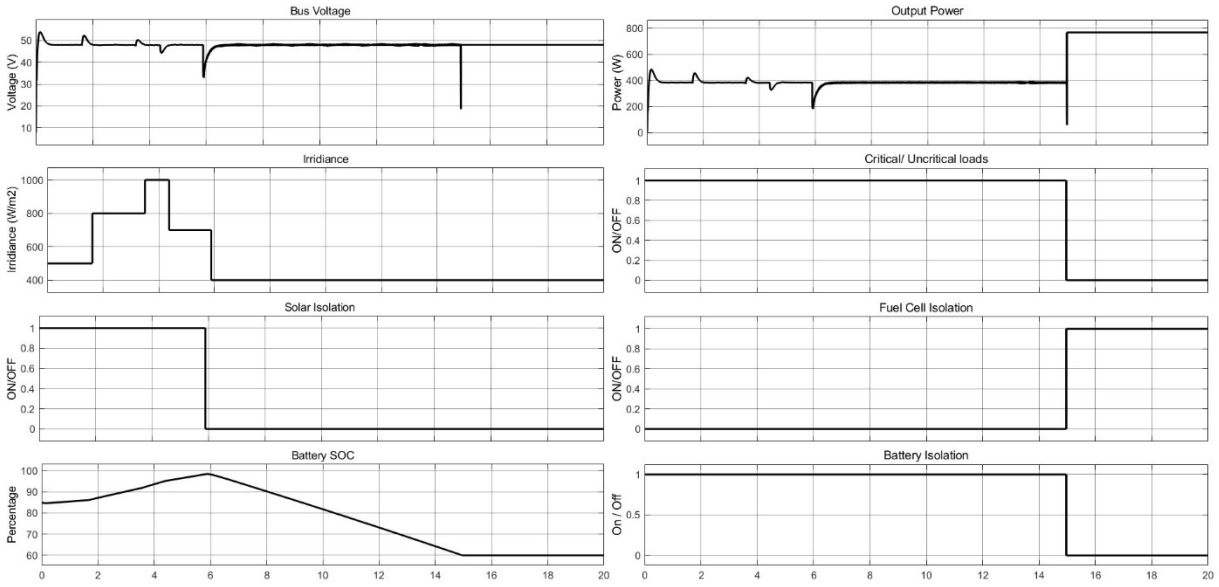

Figure 5.8. Complete simulation results with load clipping

5.7 Load variation on system performance

The impact of load variation on the microgrid is illustrated in Figure 5.9. The observed DC bus voltage across the load is ±48V DC shown in Figure 5.9A. The resultant output power ranges from ±1500W to ±400W as the load is increased as shown in Figure 5.9 E. The bus voltage remained relatively constant as the bus current decreased due to the load manipulation. It is observed in Figure 5.9C that as the load resistance is increased, the bus current and output power decreased as shown in Figure 5.9D and Figure 5.9E, while the bus voltage was stable at ±48V DC. Conversely, a decrease in load resistance means there is a smaller number of users on the microgrid, the energy resources can supply power without experiencing any strain as its can be seen in Figure 5.9E. As the number of users increases, the energy source fails to keep up with the demands. so being able to have direct control on the consumers that are connected to the grid. means that we can schedule some appliances when there is sufficient power available as the number of users or consumers decreases. More power becomes available for other appliances to be connected back to the grid. This observation illustrates the impact of load scheduling, highlighting the potential to power only essential appliances when the microgrid energy consumption is high, thereby allowing efficient microgrid energy utilization. Implementing this approach would result in a consistent output power curve without significant peaks or lows.

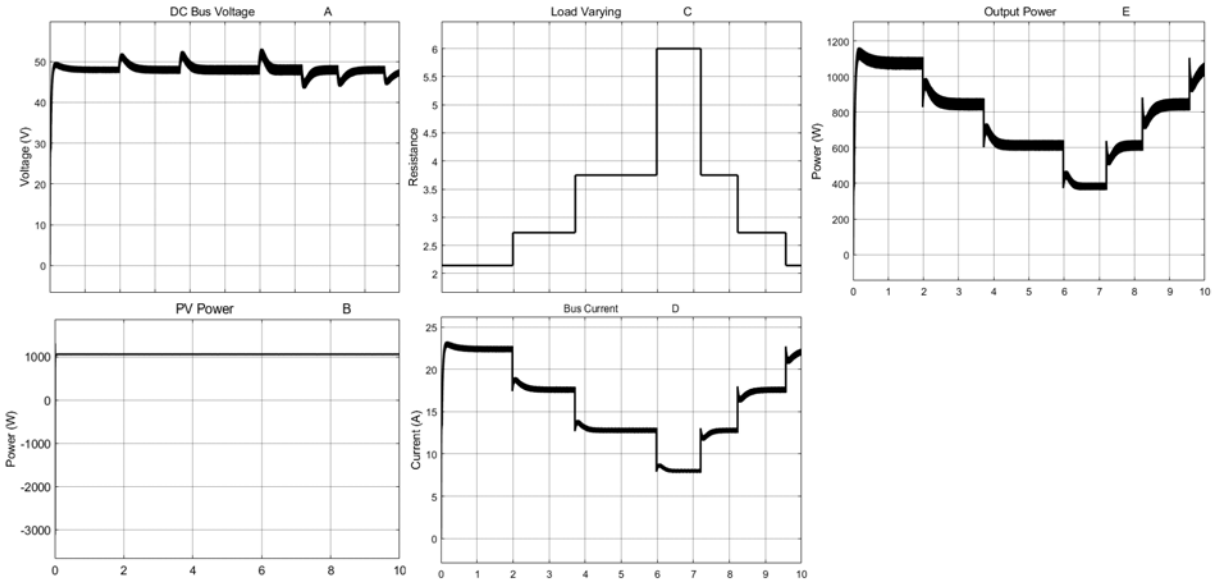

Figure 5.9. Load varying effects on the system.

5.8 Chapter summary

Chapter 5 presents the results for the simulations conducted in this study. The effect of having control on the demand side is shown. Without demand side management, the grid would experience substantial strain which would result in microgrid output power failure. Allowing load control ensures that the microgrid operates under optimal conditions which ultimately prevents system strain.

Conclusion

6.1 Summary

DC microgrid has great potential in South Africa to provide rural electrification. Considerable research has been conducted on renewable energy to migrate from the use of fossil fuels and move to clean energy. The scope of this study was to design, model and simulate a DC microgrid that would meet the consumers' energy demand in a typical rural environment. The primary objective of the study was to optimize the microgrid to ensure continuous power supply to the consumer. This involved the implementation of an MPPT to maximize power obtained from the PV for load optimal load distribution and battery charging. A bidirectional buck boost converter was used for the battery management system, along with a PI controller for battery charging and discharging control. In the event of a failure between the battery and PV, the fuel cell directly supplied the load. These three components were controlled individually, and a switching algorithm was implemented in MATLAB® to safeguard the microgrid by allowing the remaining components to sustain load supply in the event of component downtime. The switching algorithm considered irradiance and battery state of charge to anticipate which component should be activated.

The DC microgrid was designed in chapter 3 based on the energy usage in Table 3.1. The components which made up the microgrid were the PV, fuel cell and battery, these components were selected based on the selected location weather conditions. Sizing calculation was then performed to size the PV, battery and fuel cell. The calculated values were then compared to HOMER software application, which is an application for sizing renewable energy sources and give approximated cost. This comparison played a huge role in ensuring the accurateness of the sized components and the obtained results were very close to each other. The DC microgrid was then modeled based on the design calculations in chapter 3. The modelling started with a solar cell mathematical modelling based on solar cell circuit diagram. The modelled solar cell results were then compared to a PV block that exist in MATLAB. The comparison was done under the same simulation condition, the current and voltage behavior was observed and presented in the results sections. After the modelling of solar cell, an analysis on boost convertor was done in 3 approaches first one being the use of equations, there after using state space and

lastly the transfer function. Chapter 4 concluded by the simulation of a complete model which consisted of the 3 energy sources and a control strategy.

The results outlined in chapter 5 compared a microgrid without a demand side control strategy to one with such a strategy. The comparison revealed that the demand side management system enables consumers to power essential appliances during adverse weather conditions. Implementing demand-side management could potentially reduce the impact of load shedding in South Africa. Currently, when the national grid experiences excessive strain in a specific location, the entire area is subject to shut down. However, with demand-side management strategies, only specific appliances are shut down, while critical appliances remain operational, as depicted in chapter 5, figure 5.8. The implementation of load scheduling enhanced microgrid operation by relieving strain during periods of high consumer demand.

At any time of the simulation, the microgrid was able to supply the consumers with power. There were some deeps in supplied voltage as observed in figure 5.7, this was due to that small switching period between sources and could be easily neglected as it is very short period. A properly sized DC microgrid, along with appropriate energy management strategies and energy components tailored to the location weather conditions, can meet the energy requirements of rural and informal settlements.

6.1.1 Recommendations

Algorithms were developed using MATLAB™ function to safeguard the microgrid by allowing the remaining component to sustain load supply in case of one or two component failures, such as during planned maintenance or unforeseen faults. The switching algorithm considered irradiance and battery state of charge to anticipate which component should be activated. To run this algorithm high efficiency laptops are recommended.

6.1.2 Future work

The future work of the thesis would be to do an economic analysis on implementing such a microgrid and a small-scale DC microgrid based on the design, as well as compare the obtained

simulation results with the constructed microgrid. The economic analysis would be very crucial because the battery life cycle is very short and the cost of running a fuel cell is very expensive as it's a new technology. This analysis would help in determining if it is feasible to invest in such a microgrid and how long it would take for the microgrid to pay the return on investment.

References

[1] G. Prinsloo, R. Dobson, and A. Mammoli, "Smart Village Load Planning Simulations in Support of Digital Energy Management for Off-grid Remote Rural Community Microgrids," *Current Alternative Energy, Special Issue on Standalone Renewable Energy Systems for Remote Area Power Supply,* vol. 2, pp. 1-29, 01/22 2018, doi: 10.2174/2405463102666171122161858.

[2] N. Jamal, "Options for the supply of electricity to rural homes in South Africa," *Journal of Energy in Southern Africa,* vol. 26, pp. 58-65, 08/01 2015, doi: 10.17159/2413-3051/2015/v26i3a2129.

[3] R. Matsheta and I. Sefoka, "Load-Shedding in South Africa: An Immediate Threat to the Right to Education, "Section 29 Inquiry"," *Journal of Educational and Social Research,* vol. 13, p. 216, 01/05 2023, doi: 10.36941/jesr-2023-0020.

[4] M. Nowakowska and A. Tubis, "Load shedding and the energy security of Republic of South Africa," *Journal of Polish Safety and Reliability Association,* vol. 6, 10/01 2015.

[5] M. Choli, "Carbon dioxide in emissions a power system model: A case study of Germany and Poland," Masters Research, Joint Nordic Master's Programme in the

Innovative Sustainable Energy Engineering, track Energy Systems, KTH Royal Institute of Technology, 2019.

[6] M. Mansoor, B. Wang, and A. Haider, "Nonrenewable energy—environmental and health effects on human capital: empirical evidence from Pakistan," *Environmental Science and Pollution Research,* vol. 27, pp. 1-17, 01/01 2020, doi: 10.1007/s11356-019-06686-7.

[7] M. F. Zia, E. Elbouchikhi, and M. Benbouzid, "Microgrids energy management systems: A critical review on methods, solutions, and prospects," *Applied Energy,* vol. 222, pp. 1033-1055, 2018/07/15/ 2018, doi: https://doi.org/10.1016/j.apenergy.2018.04.103.

[8] A. Densmore and G. Prasad, *An Energy Market for Rural, Islanded Micro-grids*. 2015.

[9] M. Zachar and P. Daoutidis, "Understanding and predicting the impact of location and load on microgrid design," *Energy,* vol. 90, 08/01 2015, doi: 10.1016/j.energy.2015.08.010.

[10] G. Blomquist, "The Effect of Electric Utility Power Plant Location on Area Property Value," *Land Economics,* vol. 50, no. 1, pp. 97-100, 1974, doi: 10.2307/3145233.

[11] M. M. Iqbal, S. Kumar, C. Lal, and C. Kumar, "Energy management system for a small-scale microgrid," *Journal of Electrical Systems and Information Technology,* vol. 9, no. 1, p. 5, 2022/03/15 2022, doi: 10.1186/s43067-022-00046-1.

[12] Z. Zhang, X. Yang, Z. Wang, Z. Chen, and Y. Zheng, "Highly applicable small hydropower microgrid operation strategy and control technology," *Energy Reports,* vol. 6, 10/01 2020, doi: 10.1016/j.egyr.2020.08.037.

[13] I. Kiriakos and F. Zaro, *Designing a Microgrid for a Real Grid Tied PV System*. 2021, pp. 1-11.

[14] N. P.-v. Zyl. "Eskom launches demo solar microgrid project." ESI Africa. https://www.esi-africa.com/industry-sectors/future-energy/eskom-launches-solar-microgrid-project/ (accessed 03 March, 2022).

[15] B. Zohuri, "Hybrid Renewable Energy Systems," 2018, pp. 1-38.

[16] S. Dawoud, X. Lin, and M. Okba, "Hybrid renewable microgrid optimization techniques: A review," *Renewable and Sustainable Energy Reviews,* vol. 82, 09/01 2017, doi: 10.1016/j.rser.2017.08.007.

[17] M. Ponnusamy, H. Rajaguru, and R. Singaravelu, "An Overview of Batteries for Photovoltaic (PV) Systems," *International Journal of Computer Applications,* vol. 82, pp. 28-32, 11/01 2013, doi: 10.5120/14170-2299.

[18] R. Georgious, R. Refaat, J. Garcia, and A. A. Daoud, "Review on Energy Storage Systems in Microgrids," *Electronics,* vol. 10, no. 17, p. 2134, 2021. [Online]. Available: https://www.mdpi.com/2079-9292/10/17/2134.

[19] M. A. Abdulgalil, M. Khalid, and F. Alismail, "Optimal Sizing of Battery Energy Storage for a Grid-Connected Microgrid Subjected to Wind Uncertainties," *Energies,* vol. 12, no. 12, p. 2412, 2019. [Online]. Available: https://www.mdpi.com/1996-1073/12/12/2412.

[20] V. Boscaino, R. Miceli, G. Capponi, and G. Galluzzo, "A review of fuel cell based hybrid power supply architectures and algorithms for household appliances," *International Journal of Hydrogen Energy,* vol. 39, pp. 1195–1209, 01/16 2014, doi: 10.1016/j.ijhydene.2013.10.165.

[21] F. Girbau-LListuella, F. Díaz-González, and A. Sumper, "Optimization of the Operation of Smart Rural Grids through a Novel Energy Management System," *Energies,* vol. 11, no. 1, p. 9, 2018. [Online]. Available: https://www.mdpi.com/1996-1073/11/1/9.

[22] C. Breyer *et al.*, "On the History and Future of 100% Renewable Energy Systems Research," *IEEE Access,* vol. 10, pp. 78176-78218, 2022, doi: 10.1109/ACCESS.2022.3193402.

[23] B. Sørensen, "Energy and Resources," *Science,* vol. 189, no. 4199, pp. 255-260, 1975, doi: doi:10.1126/science.189.4199.255.

[24] A. B. Lovins, "Long-term Constraints on Human Activity," *Environmental Conservation,* vol. 3, no. 1, pp. 3-14, 1976, doi: 10.1017/S0376892900017641.

[25] B. Sørensen, "Scenarios for greenhouse warming mitigation," *Energy Conversion and Management,* vol. 37, no. 6, pp. 693-698, 1996/06/01/ 1996, doi: https://doi.org/10.1016/0196-8904(95)00241-3.

[26] M. Z. Jacobson and M. A. Delucchi, "Providing all global energy with wind, water, and solar power, Part I: Technologies, energy resources, quantities and areas of infrastructure, and materials," *Energy Policy,* vol. 39, no. 3, pp. 1154-1169, 2011/03/01/ 2011, doi: https://doi.org/10.1016/j.enpol.2010.11.040.

[27] G. Czisch, "Szenarien zur zukünftigen Stromversorgung, kostenoptimierte Variationen zur Versorgung Europas und seiner Nachbarn mit Strom aus erneuerbaren Energien," PHD, Kassel, Universität, FB 16, Elektrotechnik/Informatik, 2006.

[28] D. Heide, L. von Bremen, M. Greiner, C. Hoffmann, M. Speckmann, and S. Bofinger, "Seasonal optimal mix of wind and solar power in a future, highly renewable Europe," *Renewable Energy,* vol. 35, no. 11, pp. 2483-2489, 2010/11/01/ 2010, doi: https://doi.org/10.1016/j.renene.2010.03.012.

[29] M. Sterner, "Bioenergy and renewable power methane in integrated 100% renewable energy systems. Limiting global warming by transforming energy systems," *Fraunhofer IWES,* 01/01 2010.

[30] D. Bogdanov *et al.*, "Low-cost renewable electricity as the key driver of the global energy transition towards sustainability," *Energy,* vol. 227, p. 120467, 2021/07/15/ 2021, doi: https://doi.org/10.1016/j.energy.2021.120467.

[31] D. Bogdanov, A. Gulagi, M. Fasihi, and C. Breyer, "Full energy sector transition towards 100% renewable energy supply: Integrating power, heat, transport and industry sectors including desalination," *Applied Energy,* vol. 283, p. 116273, 2021/02/01/ 2021, doi: https://doi.org/10.1016/j.apenergy.2020.116273.

[32] J. N. Carl-Jochen Winter, *Hydrogen as an Energy Carrier*, 1 ed. (Technologies, Systems, Economy). Springer Berlin, Heidelberg, 2011, pp. XII, 380.

[33] C. J. W. a. J. Nitsch, *Hydrogen as an Energy CarrierTechnologies, Systems, Economy*. Germany: Springer, 1988.

[34] P. Veers *et al.*, "Grand challenges in the science of wind energy," *Science,* vol. 366, no. 6464, p. eaau2027, 2019, doi: doi:10.1126/science.aau2027.

[35] H. Holttinen *et al.*, "System Impact Studies for Near 100% Renewable Energy Systems Dominated by Inverter Based Variable Generation," *IEEE Transactions on Power Systems,* vol. 37, no. 4, pp. 3249-3258, 2022, doi: 10.1109/TPWRS.2020.3034924.

[36] S. Salkalachen, "Sun power," *Current science,* vol. 107, p. 1247, 10/25 2014.

[37] A. Goetzberger, J. Luther, and G. Willeke, "Solar cells: past, present, future," *Solar Energy Materials and Solar Cells,* vol. 74, no. 1, pp. 1-11, 2002/10/01/ 2002, doi: https://doi.org/10.1016/S0927-0248(02)00042-9.

[38] D. Sharma, R. Mehra, and B. Raj, "Comparative analysis of photovoltaic technologies for high efficiency solar cell design," *Superlattices and Microstructures,* vol. 153, p. 106861, 2021/05/01/ 2021, doi: https://doi.org/10.1016/j.spmi.2021.106861.

[39] C. M. MacKenzie, R. C. Greenblatt, and A. S. Cherdak, "Nimbus Power Systems (1960-1969)," *IEEE Transactions on Aerospace and Electronic Systems,* vol. AES-2, no. 6, pp. 26-37, 1966, doi: 10.1109/TAES.1966.4501985.

[40] A. Han. "Efficiency Of Solar PV, Then, Now And Future." https://sites.lafayette.edu/egrs352-sp14-pv/technology/history-of-pv-technology/#:~:text=Early%20silicon%20solar%20photovoltaic%20sells,increased%20while%20the%20cost%20decreased. (accessed.

[41] P. Gipe. "Austrian was First with Wind-Electric Turbine Not Byth or de Goyon." https://wind-works.org/austrian-was-first-with-wind-electric-turbine-not-byth-or-de-goyon/ (accessed 20/09, 2023).

[42] H. Allamehzadeh, "Wind energy history, technology and control," in *2016 IEEE Conference on Technologies for Sustainability (SusTech)*, 9-11 Oct. 2016 2016, pp. 119-126, doi: 10.1109/SusTech.2016.7897153.

[43] T. Dang, "Introduction, history, and theory of wind power," in *41st North American Power Symposium*, 4-6 Oct. 2009 2009, pp. 1-6, doi: 10.1109/NAPS.2009.5484084.

[44] F. Blaabjerg and K. Ma, "Wind Energy Systems," *Proceedings of the IEEE,* vol. 105, no. 11, pp. 2116-2131, 2017, doi: 10.1109/JPROC.2017.2695485.

[45] E. I. Ortiz-Rivera, A. L. Reyes-Hernandez, and R. A. Febo, "Understanding the history of fuel cells," in *2007 IEEE Conference on the History of Electric Power*, 3-5 Aug. 2007 2007, pp. 117-122, doi: 10.1109/HEP.2007.4510259.

[46] L. Giorgi and F. Leccese, "FuelCells:TechnologiesandApplications," *The Open Fuel Cells Journal,* vol. 6, 01/01 2013.

[47] E. F. Camacho and C. Bordons, "Model Predictive Control and Hybrid Systems," in *Model Predictive control*, E. F. Camacho and C. Bordons Eds. London: Springer London, 2007, pp. 289-310.

[48] J. P. T. Jis Sunny C, "An Optimal Energy Management Strategy for Standalone DC Microgrids," *INTERNATIONAL JOURNAL OF ENGINEERING RESEARCH & TECHNOLOGY (IJERT)* vol. 6, no. 04, 2017. [Online]. Available: http://dx.doi.org/10.17577/IJERTV6IS040404.

[49] D. Beriber and A. Talha, *MPPT Techniques for PV Systems*. 2013.

[50] A. Chitransh and S. Kumar, "The Different Type of MPPT Techniques for Photovoltaic System," *Indian Journal of Engineering and Materials Sciences,* vol. 1, p. 4, 11/01 2021, doi: 10.35940/ijee.A1809.111221.

[51] P. Basak, A. K. Saha, and S. Chowdhury, *Microgrid: Control techniques and modeling*. 2009, pp. 1-5.

[52] B. Saharia, J. Saharia, and B. Talukdar, *Theoretical Study on Performance Constraints of a DC-DC Boost Converter*. 2014.

[53] E. Natsheh, "Hybrid Power Systems Energy Management Based on Artificial Intelligence," 2020.

[54] C. Ghenai and M. Bettayeb, "Optimized design and control of an off grid solar PV/hydrogen fuel cell power system for green buildings," *IOP Conference Series: Earth and Environmental Science,* vol. 93, p. 012073, 11/01 2017, doi: 10.1088/1755-1315/93/1/012073.

[55] C. Ghenai and M. Bettayeb, "Grid-Tied Solar PV/Fuel Cell Hybrid Power System for University Building," *Energy Procedia,* vol. 159, pp. 96-103, 02/01 2019, doi: 10.1016/j.egypro.2018.12.025.

[56] G. Ferruzzi and G. Graditi, "Optimal Scheduling of a Microgrid under Uncertainty Condition: Management, Planning, and Policy," 2017, pp. 171-196.

[57] Y. Song, Y. Liu, S. Huang, T. Zhang, and R. Wang, "Multi-Objective Configuration Optimization for Isolated Microgrid with Mobile Energy Storage and Shiftable Load," in *2018 2nd IEEE Conference on Energy Internet and Energy System Integration (EI2)*, 20-22 Oct. 2018 2018, pp. 1-7, doi: 10.1109/EI2.2018.8582245.

[58] Z. Shuai *et al.*, "Microgrid stability: Classification and a review," *Renewable and Sustainable Energy Reviews,* vol. 58, pp. 167-179, 2016/05/01/ 2016, doi: https://doi.org/10.1016/j.rser.2015.12.201.

[59] K. S. Rajesh, S. S. Dash, R. Rajagopal, and R. Sridhar, "A review on control of ac microgrid," *Renewable & sustainable energy reviews,* vol. 71, pp. 814-819, 2017, doi: 10.1016/j.rser.2016.12.106.

[60] M. Yeshalem and B. Khan, "Microgrid Integration," 2018, pp. 51-66.

[61] A. Salam, A. Mohamed, and M. A. Hannan, "Technical Challenges of Microgrids," *ARPN Journal of Engineering and Applied Sciences,* vol. 3, pp. 64-69, 01/01 2008.

[62] T. C. Mosetlhe, O. M. Babatunde, T. R. Ayodele, and A. A. Yusuff, "Fault Analysis in a Grid-tied Microgrid System," in *2022 30th Southern African Universities Power Engineering Conference (SAUPEC)*, 25-27 Jan. 2022 2022, pp. 1-4, doi: 10.1109/SAUPEC55179.2022.9730738.

[63] G.-H. Gwon, Y.-S. Oh, D.-U. Kim, J. Han, and C.-H. Kim, *Analysis of efficiency for AC and DC load in LVDC distribution system*. 2014, pp. 12.18-12.18.

[64] M. Steiner and H. Reinold, *Medium frequency topology in railway applications*. 2007, pp. 1-10.

[65] M. d. S. Neves, M. A. Aredes, H. Khezri, E. T. H. Ida, and M. Aredes, "Advantages of grid-tied DC microgrid," in *2017 Brazilian Power Electronics Conference (COBEP)*, 19-22 Nov. 2017 2017, pp. 1-6, doi: 10.1109/COBEP.2017.8257249.

[66] F. Zhang *et al.*, "Advantages and challenges of DC microgrid for commercial building a case study from Xiamen university DC microgrid," *2015 IEEE First International Conference on DC Microgrids (ICDCM),* pp. 355-358, 2015.

[67] M. Gunasekaran, H. Mohamed Ismail, C. Bharatiraja, L. Mihet-Popa, and S. Padmanaban, "Energy Management Strategy for DC Micro Grid with Maximum Penetration of Renewable Energy Sources," *Applied Sciences,* vol. 8, 04/08 2018, doi: 10.3390/app8040585.

[68] R. A. Kaushik and N. M. Pindoriya, "A hybrid AC-DC microgrid: Opportunities & key issues in implementation," in *2014 International Conference on Green Computing Communication and Electrical Engineering (ICGCCEE)*, 6-8 March 2014 2014, pp. 1-6, doi: 10.1109/ICGCCEE.2014.6922391.

[69] H. Krishnamoorthy, P. Enjeti, S. Ahmed, and I. Pitel, *Medium voltage power distribution architecture with medium frequency isolation transformer for data centers*. 2014, pp. 3485-3489.

[70] K. Mikhaylov, J. Tervonen, and D. Fadeev, "Development of Energy Efficiency Aware Applications Using Commercial Low Power Embedded Systems," 2012.

[71] B. Dong, Y. Li, Z. Zheng, and L. Xu, "Control strategies of microgrid with Hybrid DC and AC Buses," 01/01 2011.

[72] X. Jianfang, W. Peng, L. Setyawan, C. Jin, and F. Choo, *Energy management system for control of hybrid AC/DC microgrids*. 2015, pp. 778-783.

[73] K. Muralidhar and N. Rajasekar, "A new design and feasible architecture of DC microgrid for rural electrification," *International Transactions on Electrical Energy Systems,* vol. 31, no. 8, p. e12973, 2021, doi: https://doi.org/10.1002/2050-7038.12973.

[74] Y. C. C. Wong, C. S. Lim, M. D. Rotaru, A. Cruden, and X. Kong, "Consensus Virtual Output Impedance Control Based on the Novel Droop Equivalent Impedance Concept for a Multi-Bus Radial Microgrid," *IEEE Transactions on Energy Conversion,* vol. 35, no. 2, pp. 1078-1087, 2020, doi: 10.1109/TEC.2020.2972002.

[75] D. Kumar, F. Zare, and A. Ghosh, "DC Microgrid Technology: System Architectures, AC Grid Interfaces, Grounding Schemes, Power Quality, Communication Networks, Applications and Standardizations Aspects," *IEEE Access,* vol. PP, pp. 1-1, 04/18 2017, doi: 10.1109/ACCESS.2017.2705914.

[76] D. Kumar, F. Zare, and A. Ghosh, "DC Microgrid Technology: System Architectures, AC Grid Interfaces, Grounding Schemes, Power Quality, Communication Networks, Applications, and Standardizations Aspects," *IEEE Access,* vol. 5, pp. 12230-12256, 2017, doi: 10.1109/ACCESS.2017.2705914.

[77] Y. Fei, J. Zhuang, G. Li, L. Yao, and B. Yang, "Research on the dual-terminal ring topology-based dc microgrid system," *The Journal of Engineering,* vol. 2019, 03/01 2019, doi: 10.1049/joe.2018.8764.

[78] S. Pang, B. Nahid-Mobarakeh, s. Pierfederici, Y. Huangfu, G. Luo, and F. Gao, *DC Microgrid Topologies and Stability Analysis for Electrified Transportation Systems*. 2018, pp. 1055-1060.

[79] T. Ma, M. Cintuglu, and O. Mohammed, "Control of Hybrid AC/DC Microgrid Involving Storage, Renewable Energy and Pulsed Loads," *IEEE Transactions on Industry Applications,* vol. PP, pp. 1-1, 09/27 2016, doi: 10.1109/TIA.2016.2613981.

[80] S. Augustine, J. Quiroz, M. Reno, and S. Brahma, *DC Microgrid Protection: Review and Challenges*. 2018.

[81] C. Patrao, A. de Almeida, B. Harrison, B. Schlomann, M. Damnics, and P. Fonseca, "Low power mode energy demand of household appliances—SELINA and APP projects," *Energy Efficiency,* vol. 10, 10/01 2017, doi: 10.1007/s12053-017-9518-3.

[82] B. Morrow and S. Kanakri, "The impact of fluorescent and led lighting on students attitudes and behavior in the classroom," 12/01 2018, doi: 10.24105/apr.2018.5.15.

[83] M. Askarpour, J. Aghaei, M. Hassan Khooban, M. Shafie-khah, and J. P. S. Catalão, "Voltage control of critical and non-critical loads in distribution networks with electric spring," *Electric*

Power Systems Research, vol. 177, p. 105988, 2019/12/01/ 2019, doi: https://doi.org/10.1016/j.epsr.2019.105988.

[84] V. Serifi and V. Sofiu, *AN OVERVIEW OF DIRECT SOLAR IRRADIATION*. 2011.

[85] A. R. a. profileSOLAR.com. "Solar PV Analysis of Pietermaritzburg, South Africa." https://profilesolar.com/locations/South-Africa/Pietermaritzburg/ (accessed.

[86] S. A. K. .J Neil Ross, *in McEvoy's Handbook of Photovoltaics* 3ed. 2018.

[87] M. Elzalik, F. Mustafa, and R. Mostafa, "Study Of Maximum Power Point Tracking (MPPT) In PV Systems," vol. 4, pp. 18-26, 10/11 2016.

[88] J. Nedumgatt, K. Jayakrishnan, U. Subramaniam, D. Vijayakumar, and D. P. Kothari, "Perturb and observe MPPT algorithm for solar PV systems-modeling and simulation," 12/01 2011, doi: 10.1109/INDCON.2011.6139513.

[89] M. Hebchi, K. Abdellah, and C. Abdelghani, "Improved perturb and observe algorithm for maximum power point tracking in a photovoltaic system," *EEA - Electrotehnica, Electronica, Automatica,* vol. 66, pp. 5-14, 10/01 2018.

[90] M. Biswal and S. Sabyasachi, "A Study on Recent DC-DC Converters," *International Journal of Engineering Research and Applications (IJERA),* vol. 2, pp. 657-663, 11/01 2012.

[91] R. L. S. Libby, L. G. Sison, and M. dela Cruz, "Switching performance characterization of SiC Schottky diodes in switch-mode DC-DC converters," 2004.

[92] S. Lopa, S. Hossain, M. Hasan, and T. Chakraborty, "Design and Simulation of DC-DC Converters," *International Research Journal of Engineering and Technology,* vol. 3, pp. 62-70, 01/24 2016.

[93] K. Mallon, F. Assadian, and B. Fu, "Analysis of On-Board Photovoltaics for a Battery Electric Bus and Their Impact on Battery Lifespan," *Energies,* vol. 10, p. 943, 07/07 2017, doi: 10.3390/en10070943.

[94] A. Hariprasad, I. Priyanka, R. Sandeep, and O. Ravi, "Battery Management System in Electric Vehicles," *International Journal of Engineering Research and,* vol. V9, 05/23 2020, doi: 10.17577/IJERTV9IS050458.

[95] M. Lawder *et al.*, "Battery Energy Storage System (BESS) and Battery Management System (BMS) for Grid-Scale Applications," *Proceedings of the IEEE,* vol. 102, pp. 1014-1030, 06/01 2014, doi: 10.1109/JPROC.2014.2317451.

[96] V. Boscaino, A. Messina, R. Miceli, and G. Capponi, "Fuel cells for household appliances: Experimental test of power management algorithms," in *2013 International Conference on Clean Electrical Power (ICCEP)*, 11-13 June 2013 2013, pp. 620-627, doi: 10.1109/ICCEP.2013.6586950.

[97] A. Kampker, H. Heimes, M. Kehrer, S. Hagedorn, P. Reims, and O. Kaul, "Fuel cell system production cost modeling and analysis," *Energy Reports,* vol. 9, pp. 248-255, 2023/03/01/ 2023, doi: https://doi.org/10.1016/j.egyr.2022.10.364.

[98] P. Dongbaare, S. O. Osuri, and S. P. Daniel Chowdhury, "A smart energy management system for residential use," 2017.

[99] J.-H. Hong, D.-Y. Hong, L.-H. Yao, and L.-C. Fu, "A Demand Side Management with Appliance Controllability Analysis in Smart Home," 2020.

Appendix A: MPPT algorithm code

```
function D = fcn (Vpv, Ipv)

%#codegen

persistent Dprev Vprev Pprev

if isempty (Dprev)

   Dprev = 0,7.

   Pprev = 2000.

   Vprev = 190.

end

 deltaD = 125e-6.

 Ppv = Vpv*Ipv.

 if (Ppv - Pprev) ~= 0

    if (Ppv - Pprev)> 0

    if (Vpv - Vprev) > 0

       D = Dprev - deltaD.

    else

       D =Dprev + deltaD.

    end

   else

       if (Vpv - Vprev)>0
```

```
            D = Dprev + deltaD.
        else
      D = Dprev - deltaD.
        end
    end
 else
    D = Dprev.
 end
 Dprev = 0.
Vprev = Vpv.
Pprev = Ppv.
function [solar, battery, FuelCells] = fcn (switchS, switchB)
solar = 0.
battery = 0.
FuelCells = 0.
if (switchS >= 500)
   solar = 1.
   battery = 1.
   FuelCells = 0.
end
```

```
if (switchB >=99)
   battery = 0.
end
if (switchS < 500 && switchB >=90)
   solar = 0.
   battery = 1.
   FuelCells = 0.
end
if (switchS <500 && switchB <90)
   solar = 0.
   battery = 0.
   FuelCells =1.
End
```

Appendix B:Simulink® model of reverse saturation equation

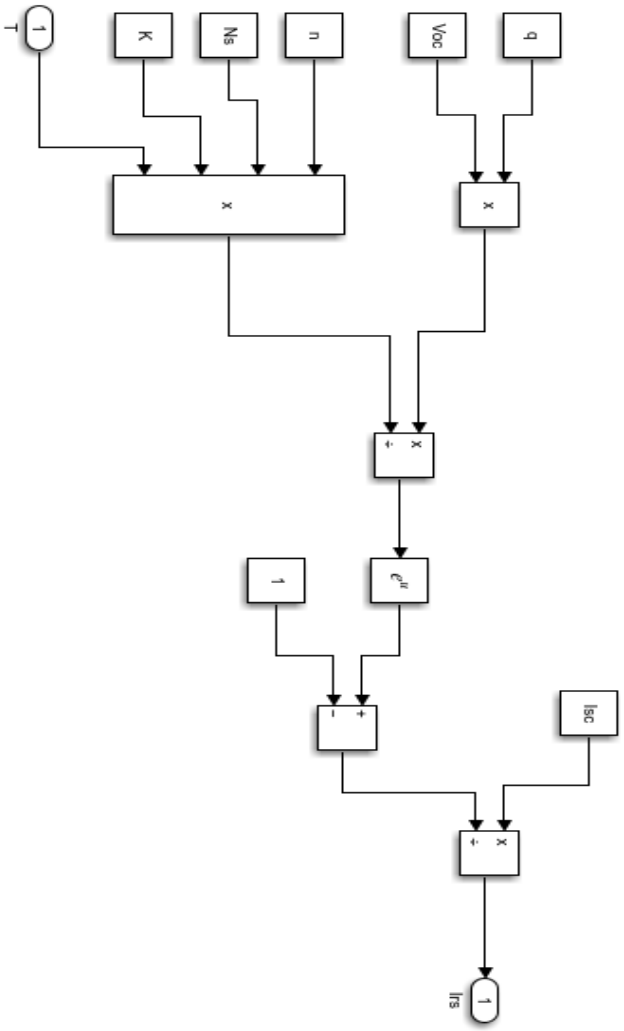

Appendix C: Model of saturation current

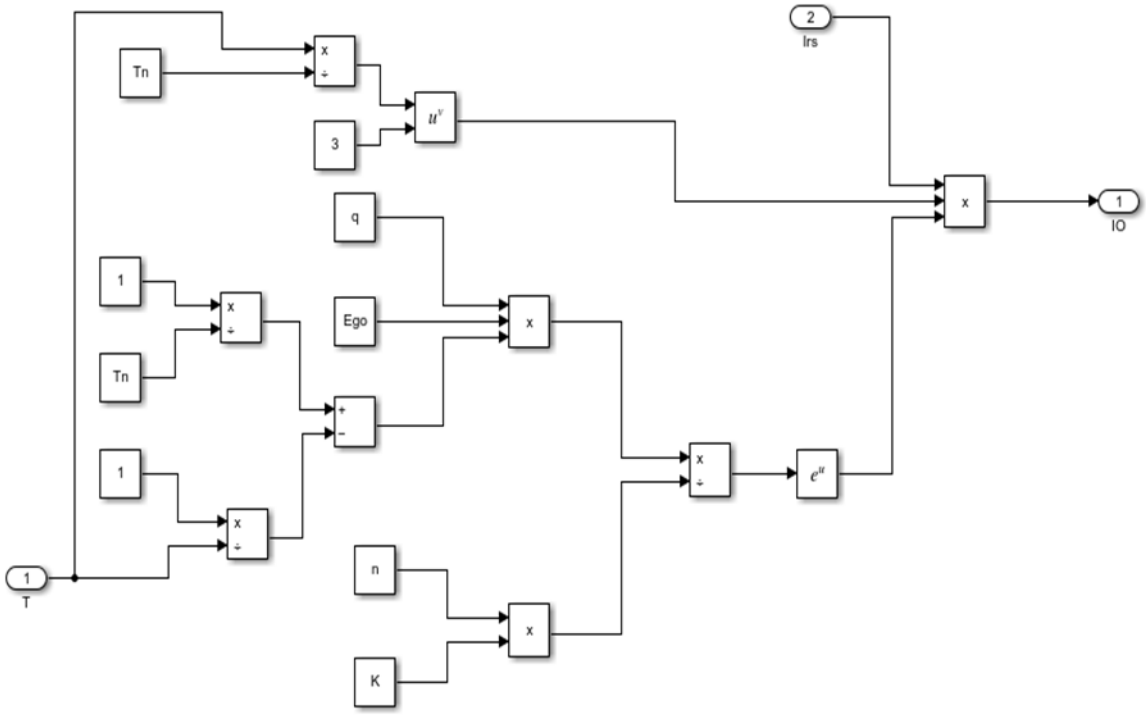

Appendix D: Model of photo current

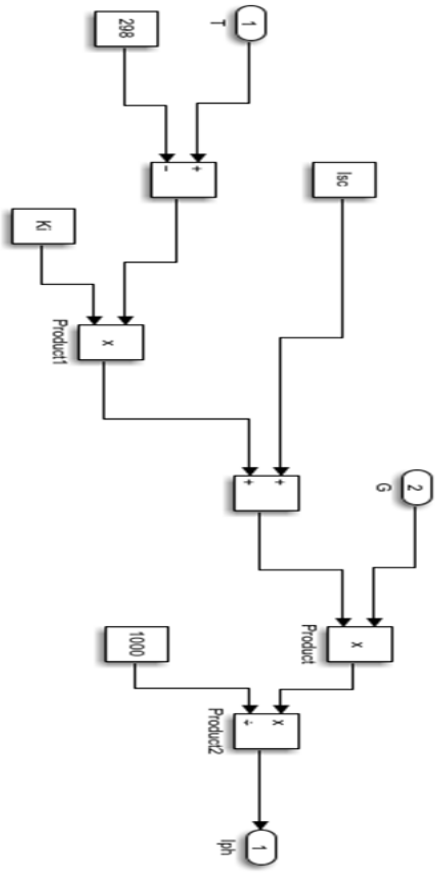

Appendix E:Model of shunt current

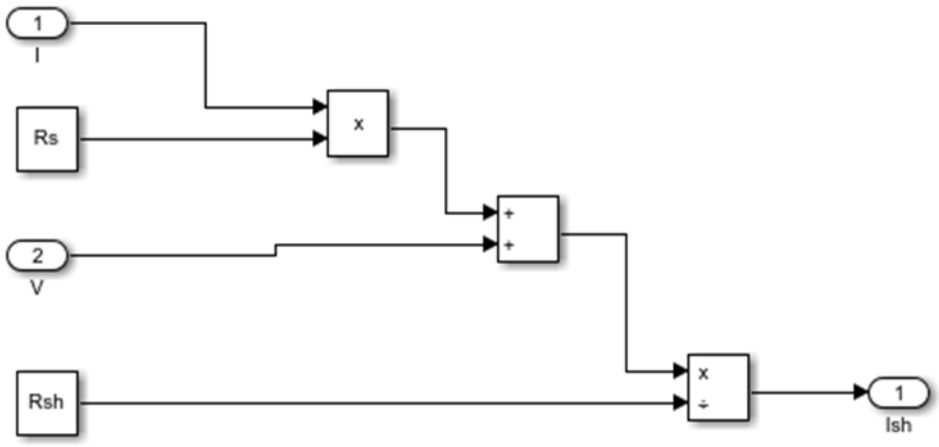

Appendix F:Output current model

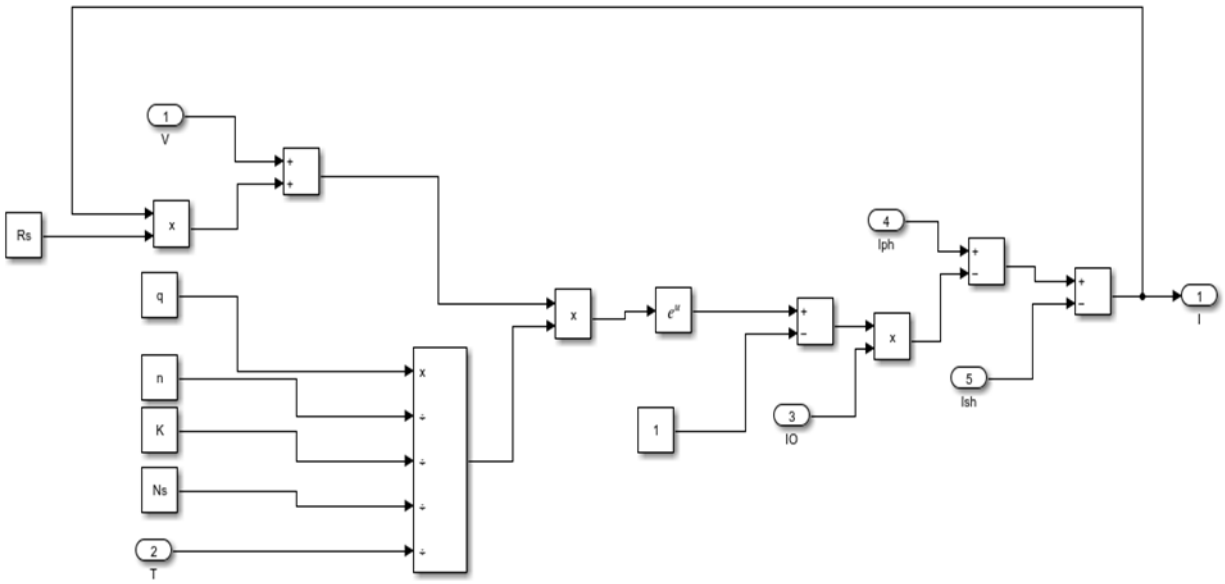

Appendix G:Solar cell model

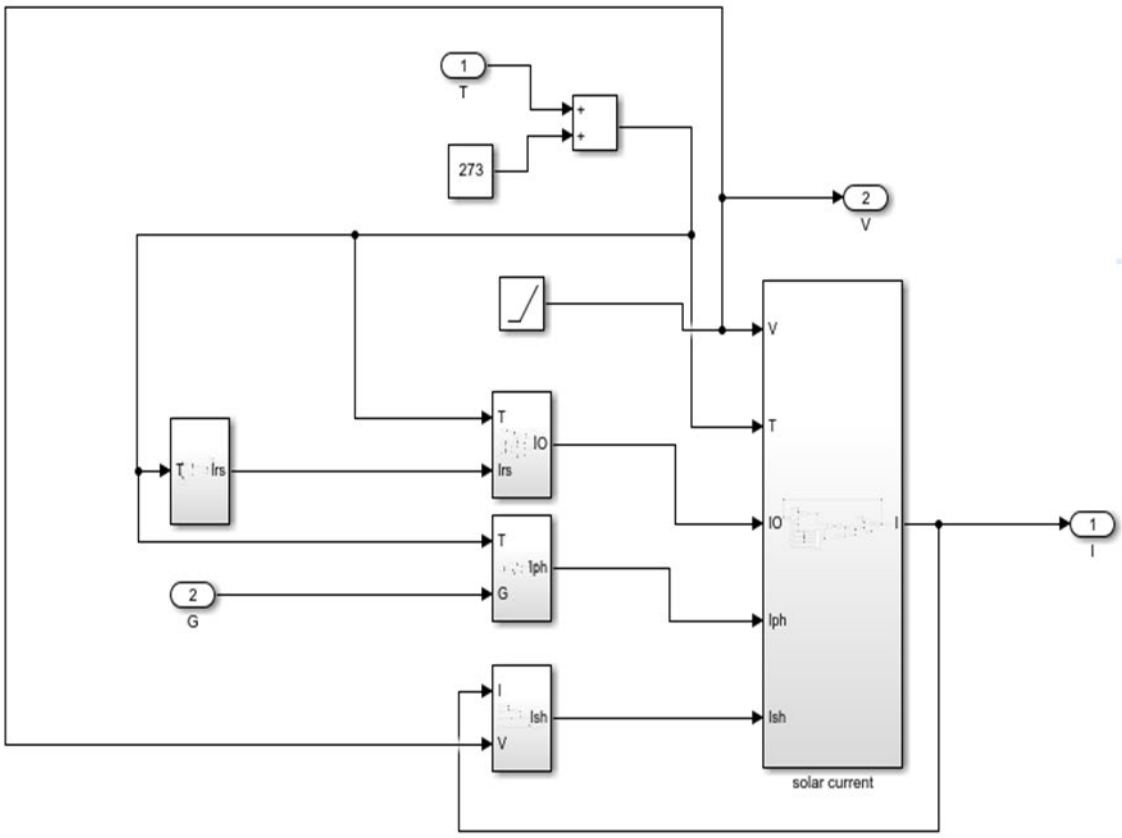

Appendix H:Solar cell simulation diagram